ELSEVIER

Journal of Structural Geology 30 (2008) 580–601

JOURNAL OF STRUCTURAL GEOLOGY

www.elsevier.com/locate/jsg

Mohr-cyclides, a 3D representation of geological tensors: The examples of stress and flow

Sara Coelho*, Cees Passchier

Department of Earth Sciences, University of Mainz, Becherweg 21, 55099 Mainz, Germany

Received 18 June 2007; received in revised form 9 December 2007; accepted 10 January 2008
Available online 17 January 2008

Abstract

Mohr-circles are commonly used to represent second-rank tensors in two dimensions. In geology, this mainly applies to stress, flow, strain and deformation. Three-dimensional second rank tensors have been represented by sets of three Mohr-circles, mainly in the application of stress. This paper demonstrates that three-dimensional second rank tensors can in fact be represented in a three-dimensional reference frame by Mohr surfaces, which are members of the cyclide family. Such Mohr-cyclides can be used to represent any second rank tensor and are exemplified with the stress and flow tensors.

Keywords: Mohr circle; Mohr cyclide; Stress; Flow; Kinematics; Tensor

1. Introduction

1.1. Historical background

Mohr diagrams, one of the most used and useful tools in structural geology, were introduced by German scientist Otto Mohr (1882). As a civil engineer, Mohr was especially interested in mechanical forces acting on planes and, thus, presented the scientific community with a graphical representation for three-dimensional stress, plotting normal stress (σ_n) versus shear stress (τ). The result was the familiar Mohr diagram for stress, consisting of the three principal circles of stress and the surface they encompass, where any plane P can be plotted and assigned values for σ_n and τ, with their orientation given in terms of single or double angles. This graphical representation has since been used extensively in empirical mechanical problems, either using failure envelopes or as a tool to study fracture opening and reactivation (e.g. Delaney et al., 1986; Jolly and Sanderson, 1997).

The Mohr-circle concept was adapted for strain tensors by Nadai (1950), who devised a graphical representation of quadratic elongation versus shear strain, where angles between lines are plotted in the unstrained form. The plot is in all ways similar to Mohr's diagram and establishes a parallel between the principal circles of stress and the principal sections of the deformation ellipse. Nadai (1950) also defined a Mohr diagram for reciprocal strain, with reciprocal quadratic elongation versus reciprocal shear strain.

Mohr diagrams were formally introduced to structural geology by Brace (1961), who coined the term and explored its multiple applications in the study of deformed rocks. This new line of research was not lost and Ramsay (1967) further demonstrated the relevance of Mohr diagrams in strain analysis, showing that Mohr circles for reciprocal strain could be used to represent strain ellipses. Means (1982) introduced the Mohr diagram for the stretch tensor, where he explored the potential of polar coordinates and its applications to the study of material line behaviour, encompassing both rotational characteristics and stretch. Further research developed numerous applications of Mohr diagrams for strain to structural geology problems, namely inhomogeneous deformation (Means, 1983), strain refraction (Means, 1983; Treagus, 1983), strain

* Corresponding author. Department of Psychology, University of Bath, Bath BA2 7AY, UK.
E-mail address: sarasscoelho@yahoo.co.uk (S. Coelho).

0191-8141/$ - see front matter © 2008 Elsevier Ltd. All rights reserved.
doi:10.1016/j.jsg.2008.01.003

analysis (Treagus, 1986 (which includes a comprehensive background on the history of Mohr diagrams in Structural Geology); Lisle and Ragan, 1988; Passchier, 1990a; Treagus, 1990; Simpson and De Paor, 1993; Vissers, 1994; Zhang and Zheng, 1997) and vorticity analysis (Passchier and Urai, 1988; Passchier, 1990b). Mohr diagrams for flow (velocity gradient) tensors were introduced by Lister and Williams (1983), following an idea of J.P. Platt. Since then, works like Means (1983), Bobyarchick (1986), Passchier (1986, 1987, 1988, 1993), Wallis (1992), Simpson and De Paor (1993) showed how these diagrams could be used to interpret and understand the principles of progressive deformation.

1.2. Tensors and Mohr-circles

As demonstrated first by Otto Mohr (1882), all tensors can be represented by Mohr diagrams. The relationship between a tensor $\mathbf{T_{ij}}$ and its Mohr-circle can be illustrated with a second-rank tensor, which requires four components (Fig. 1). In a 2D Mohr space, the vertical axis $\mathbf{T_{ij}}$ is used to plot tensor components T_{12} and T_{21}, whereas horizontal coordinates stand for the T_{ii} components, T_{11} and T_{22}. Thus, two points can be plotted (Means, 1982): x_1 as (T_{11}, $-T_{21}$) and x_2 as (T_{22}, T_{12}). Either the T_{12} or the T_{21} sign has to be changed from the original tensor components to insure equivalence of positions above or below the horizontal axis of the Mohr diagram. The convention of Means (1982) considers $-T_{21}$, and defines Mohr-diagrams of the *first kind* (De Paor and Means, 1984). If, on the other hand, one considers $-T_{12}$, the Mohr-diagram is said to be of the *second kind* (De Paor and Means, 1984). Points x_1 and x_2 define a diameter (dashed line) of a circle, which represents the Mohr-circle of tensor $\mathbf{T_{ij}}$ (Fig. 1). Any given tensor can be described by an infinite number of sets of $\mathbf{T_{ij}}$ components, each representing a description of the tensor in a specific reference frame. Considering all these possible sets, a Mohr circle can be defined as "(…) *the geometrical locus of all possible sets of tensor components*" (Means, 1992).

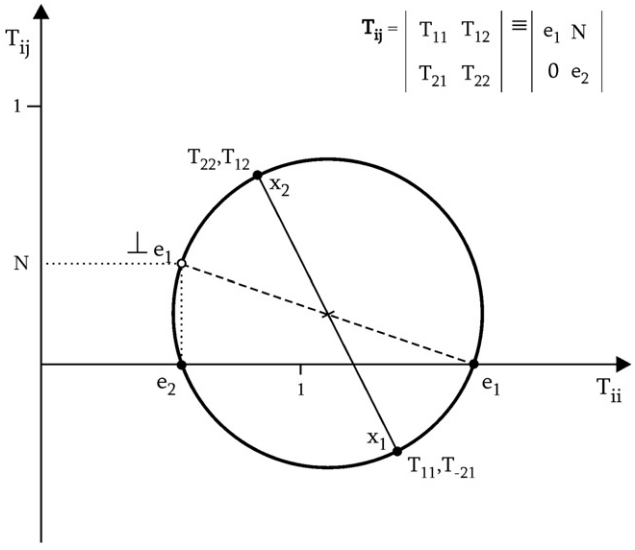

Fig. 1. Mohr-circle for an unspecified tensor $\mathbf{T_{ij}}$, defined by two alternative diameters: solid: using random tensor components; dashed: using the eigenvalues e_1 and e_2.

Second-rank tensors in three dimensions, with nine components, can also be represented by Mohr-circles. The easiest way to do this is to consider only part of the full tensor. An example of this "technique" is the literature published on velocity gradient tensors, which, for Mohr-diagram purposes, simplifies flow to monoclinic geometries, characterised by the vorticity vector parallel to one of the eigenvectors and one of the instantaneous stretching axes. Assuming this, a tensor

$$T_{ij} = \begin{vmatrix} T_{11} & T_{12} & 0 \\ T_{21} & T_{22} & 0 \\ 0 & 0 & T_{33} \end{vmatrix}$$

can be reduced to

$$T_{ij} = \begin{vmatrix} T_{11} & T_{12} \\ T_{21} & T_{22} \end{vmatrix}$$

and plotted straightforward as a Mohr-circle, ignoring the three-dimensional component given by T_{33}. A second method was suggested by Otto Mohr himself, for the case of stress, applied later to quadratic deformation. The stress (deformation) tensor is written as a diagonal matrix, where T_{ii} are the eigenvectors of the tensor and the principal stresses $\sigma_1,\sigma_2,\sigma_3$ (for instance Fig. 3), or the principal quadratic elongations $\lambda_1,\lambda_2,\lambda_3$. These components are then used to draw three circles, or half-circles, that represent the principal sections of the stress or finite strain ellipsoid.

1.3. Scope

However ingenious, Mohr-circles for second-rank tensors remain simplifications because Mohr-space is always considered to be two-dimensional. This means that in order to accommodate a three-dimensional second-rank tensor in Mohr-space, it must be partitioned into three two-dimensional second-rank tensors, resulting in a combination of three Mohr-circles. In other words, the so called "three-dimensional diagram" for stress is, in fact, a two-dimensional representation of three eigenvector sections of a second-rank symmetric tensor.

The purpose of this paper is to investigate the possibility of expanding the representation of tensors into a three-dimensional Mohr-space, using examples of stress and flow. After some initial testing, it turned out that real three-dimensional Mohr-diagrams do exist and are represented by surfaces of the cyclide family and related toroids. These surfaces share all the useful properties of 2D Mohr-diagrams, with the advantage of a full three-dimensional geometry. They will be henceforth referred to as *Mohr-cyclides*. Symbols and conventions are listed in Appendix A.

1.4. Some properties of cyclides

A general cyclide is a non-spherical fourth degree polynomial surface, introduced by Dupin (1822), which can be defined by an implicit equation:

$$\left(x^2+y^2+z^2-D^2+B^2\right)^2=4(Ax-CD)^2+4(By)^2 \quad (1)$$

or a parametric system (e.g. Pratt, 1990; Fig. 2a):

$$x=\frac{B\sin\psi(C\cos\theta-D)}{A-C\cos\theta\cos\psi}$$

$$y=\frac{D\left(C-A\cos\theta\cos\psi\right)+B^2\cos\theta}{A-C\cos\theta\cos\psi} \quad \text{with} \quad \begin{matrix}\theta\geq 0^\circ\\ \psi\leq 180^\circ\end{matrix}$$

$$z=\frac{B\sin\theta(A-D\cos\psi)}{A-C\cos\theta\cos\psi} \quad (2)$$

where A, B, C and D are constant parameters, with $B^2=A^2-C^2$. The relative magnitude of parameters A, C and D (B is always dependent) defines the shape of the surface in the cyclide family (Fig. 2; Shene, 2000). This work will focus mainly on single-crescent cyclides and torii with converging points. Some other cyclide properties are (Allen and Dutta, 1997; Shene, 2000; Fig. 2):

(1) All lines on the curvature of the cyclide, defined by equal values of θ or ψ, are circles.
(2) A cyclide has two orthogonal planes of symmetry.
(3) The cyclide is fully defined by four major circles, two in each symmetry plane, given by: $\theta=0^\circ$, $\theta=180^\circ$, $\psi=0^\circ$, $\psi=180^\circ$. If parameter D is equal to either A or C, three circles are enough.
(4) The radii of the major circles are defined by the A, C, and D parameters.

2. Mohr-cyclides for stress

2.1. Mohr-circles for stress

A stress tensor $\mathbf{S_{ij}}$ can be represented in 2D as a Mohr diagram, defined by the three major circles, which represent planes of principal stress, and the area encompassed by them (Fig. 3). The principal circles intersect the σ_n axes at three points, which correspond to the three principal axes of stress σ_1, σ_2 and σ_3 (maximum, intermediate and minimum stress). Since shear stress is zero at these orientations, σ_1, σ_2 and σ_3 also represent the eigenvalues of $\mathbf{S_{ij}}$. Normal and shear stress (σ_n and τ) values can be read as Cartesian coordinates in the σ_n- and τ-axis for any plane P, represented by its normal N_P within this area. The orientation of P with respect to the principal stresses is given by arcs of circles (dashed lines in Fig. 3). Since stress is a symmetric tensor, principal circles are centred on the σ_n-axis and, for simplification, Mohr-diagrams usually display the top half-circles only.

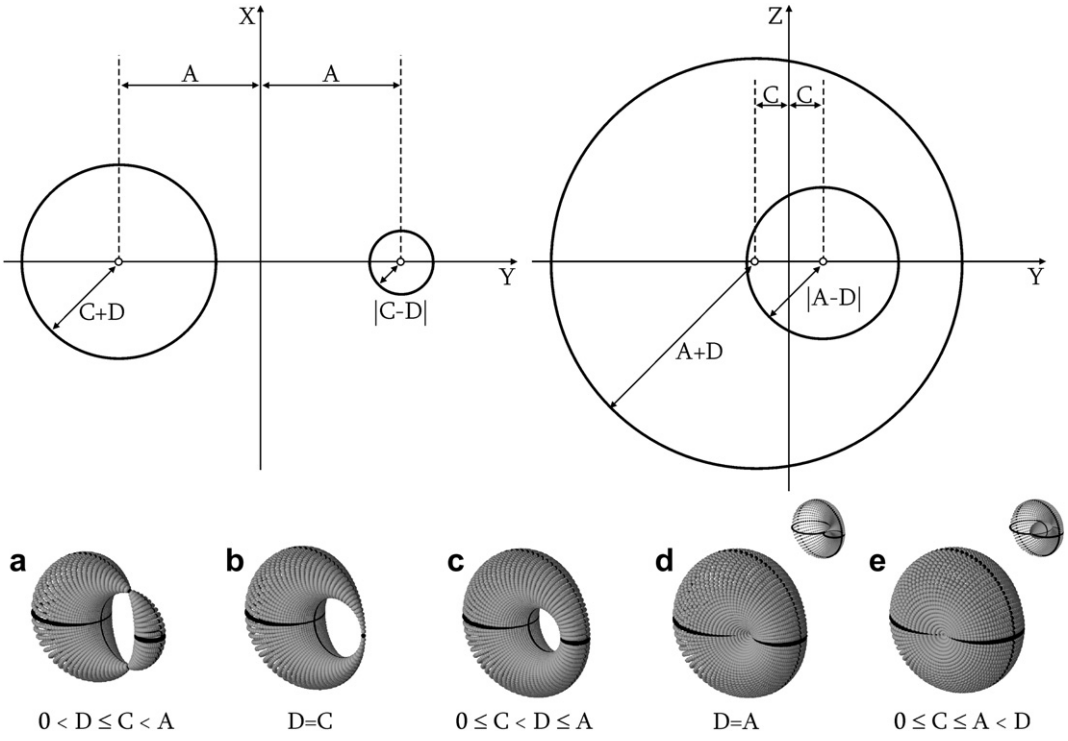

Fig. 2. A general cyclide and its parameters with thumbnails of several surfaces of the cyclide family: (a) Double-crescent cyclide; (b) single-crescent cyclide; (c) ring-cyclide (torus); (d) torus with a converging point, or, single singularity spindle-cyclide; (e) double-singularity spindle cyclide. Black lines represent the principal circles of each cyclide surface.

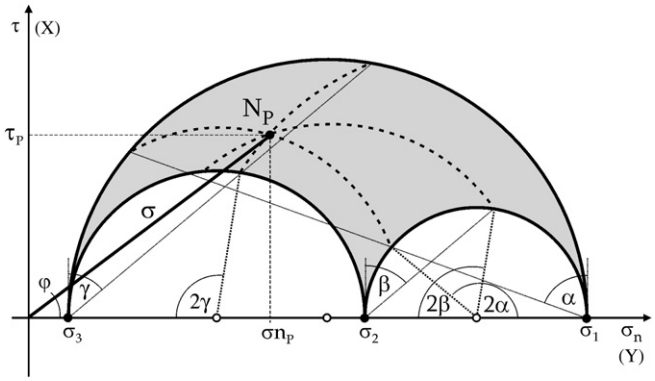

Fig. 3. A Mohr diagram for stress (lower half left out for simplicity). All possible orientations plot as poles to planes in the circle perimeter or in the shaded area. Stress components for a plane P can be read as Cartesian (σ_{nP}, τ_P) or polar ($\sigma\cos\varphi$, $\sigma\sin\varphi$) coordinates. Orientation of plane P is determined with angles α, β, γ, measured to its pole with respect to the principal stresses σ_1, σ_2, σ_3.

2.2. Plotting procedure

The stress tensor operation assigns a unique stress vector σ to each plane P. In traditional Mohr diagrams for stress, the angle between σ and the pole N_P to plane P is used to find normal and shear stress for each plane, as discussed above. However, some information is omitted with this construction method, because the angle $\sigma \wedge N_P$ can be the same for planes with different orientations in space. This implies that stress vectors for two different planes can plot at the same point in a Mohr-circle. 3D cyclide constructions in Mohr space address this problem.

Plotting $\mathbf{S_{ij}}$ in a three-dimensional space requires the definition of a second angle δ. In order to do this, it is useful to choose an inherent property of the stress tensor itself, i.e., an element that does not involve external reference frames. We consider the relative orientation of the *stress plane* S, which contains the stress vector and the pole N_P (and therefore σ, σ_n and τ), with respect to one of the eigenvectors of $\mathbf{S_{ij}}$, in this case σ_1. This is the first significant difference between 2D and 3D representations of stress, since the geometrical properties of 2D Mohr-circles unavoidably lock S in its 2D (σ_n-τ) reference frame. The angle δ is thus defined as the angle between the pole of the stress plane N_S, a line in plane P normal to τ, and the maximum principal stress σ_1 (Fig. 4a,b). δ values can be calculated using the dot-product expression:

$$N_S \cdot \sigma_1 = \overline{N}_S \cdot \overline{\sigma}_1 \cdot \cos\delta$$

$$\cos\delta = \frac{N_{Sx}\sigma_{1x} + N_{Sy}\sigma_{1y} + N_{Sz}\sigma_{1z}}{\overline{N}_S \cdot \overline{\sigma}_1} \tag{3}$$

where N_{Si}, σ_{1i} are vectorial components and the upper bar denotes magnitude. Since N_S is the pole of the stress plane, defined for example by σ_n and σ, its components are obtained via the cross-product:

$$\sigma_n \times \sigma = \det \begin{vmatrix} N_{Sx} & N_{Sy} & N_{Sz} \\ \sigma_{nx} & \sigma_{ny} & \sigma_{nz} \\ \sigma_x & \sigma_y & \sigma_z \end{vmatrix} \tag{4}$$

Since N_S is normal to τ, shear stress in P can be resolved into two components, one in the direction of σ_1, $\tau_{\sigma 1}$ and the other normal to the principal maximum stress, $\tau_{\perp\sigma 1}$ (Fig. 4b). Adding the angle δ allows the stress planes to unfold from the fixed 2D plane (YZ) and materialises a three-dimensional surface with the same properties of a Mohr diagram (Fig. 4d). The resulting shape is a single-crescent cyclide, a *Mohr-cyclide for stress*, which can be defined in polar coordinates or analytically.

The value of δ defines three cases of special significance which help to understand its geometric effect:

(1) Where $\boldsymbol{\delta = 0^\circ}$ (Fig. 4c), σ_1 lies in the P-plane and, therefore, is orthogonal to the S-plane and its components σ, σ_n and τ. It is clear that σ_2 and σ_3 will be on the S-plane and that $\alpha\ (N \wedge \sigma_1) = 90^\circ$, so $\delta = 0^\circ$ defines the $\sigma_2\sigma_3$ principal stress plane, plotted in the XY-plane of the Mohr-cyclide. In this case, there is no shear stress in the σ_1 direction ($\tau_{\sigma 1} = 0$), which is in agreement with the condition $\sigma_1 \perp \tau$.
(2) If $\boldsymbol{\delta = 90^\circ}$ (Fig. 4c), σ_1 is a line in the S-plane, normal to the P-plane. In this arrangement, α is variable and one of the minor principal stresses (either σ_2 or σ_3) is parallel to N_S. Therefore, $\delta = 90^\circ$ is a condition for the $\sigma_1\sigma_2$ and $\sigma_1\sigma_3$ principal planes of stress, which plot in the YZ-plane in Mohr space. In these planes, shear stress is zero in orientations normal to σ_1 ($\tau_{\perp\sigma 1} = 0$), in agreement with the fact that σ_1 and τ are both in S.
(3) All other scenarios, with δ in the range $]0^\circ,90^\circ[$, or, $]90^\circ,180^\circ[$ (Fig. 4b) are intermediate between the two previous conditions and account for planes oblique to the principal stress planes.

Polar coordinates of P in a Mohr-cyclide are similar to coordinates in the 2D scenario, but with the extra degree of freedom added by angle δ they become (σ, φ, δ), as shown in Fig. 4b:

$$X_M = \sigma \cdot \sin\varphi \cdot \cos\delta$$

$$Y_M = \sigma \cdot \cos\varphi$$

$$Z_M = \sigma \cdot \sin\varphi \cdot \sin\delta \tag{5}$$

The analytical description of the Mohr-cyclide follows the equations of a general cyclide (Eqs. (1) and (2)). However, Mohr-cyclides for stress represent a special case, where the simplification $C = D$ applies (Fig. 2). The parameters can be further adapted, considering the radii of the principal circles of the cyclide which represent the principal planes of stress, as shown above (Fig. 5):

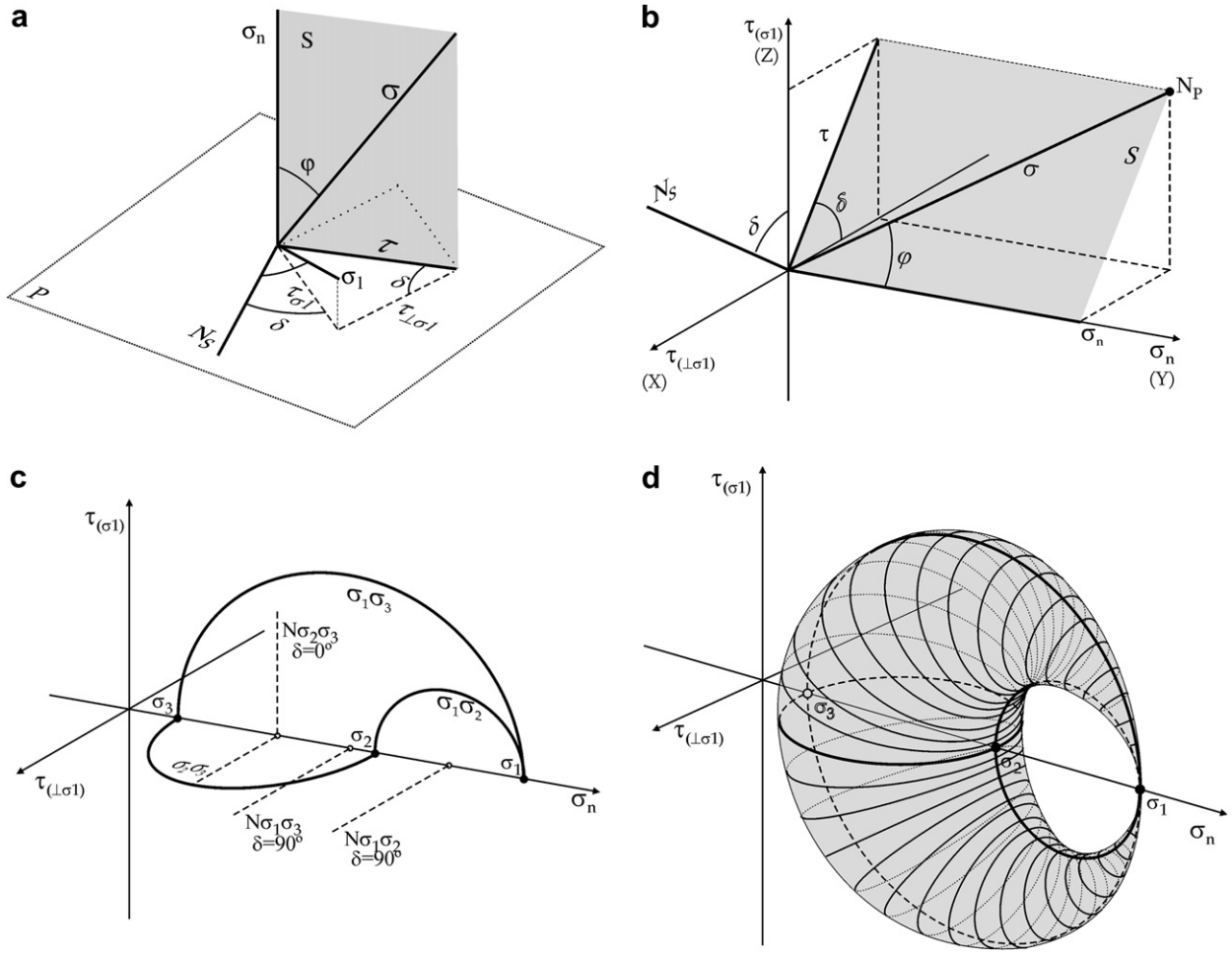

Fig 4. Mohr-cyclides for Stress. (a) Stress vectors in real space; (b) Stress vectors in 3D Mohr-space; (c) principal planes of stress in 3D (only half-circles are shown for simplicity); (d) the corresponding Mohr-cyclide, built with Eq. (5) or Eq. (8) (lines represent families of equal θ planes). Perspective changes slightly in (d).

$$A = \frac{2\sigma_1 - \sigma_2 - \sigma_3}{4}$$
$$C = \frac{\sigma_2 - \sigma_3}{4} \tag{6}$$

There is, nevertheless, one important difference: cyclides in the canonical form are centred at the origin, while stress Mohr-cyclides may not. To address this problem, it is necessary to introduce an extra parameter, called E, that shifts the Mohr-cyclide in the Y-direction. E can be found by the expression:

$$E = \sigma_1 - A = \frac{2\sigma_1 + \sigma_2 + \sigma_3}{4} \tag{7}$$

Note that E is not a translation in the physical sense, it merely allows the principal plane of the cyclide to be identical to the principal planes of stress. Substituting Eqs. (6) and (7) into Eq. (2) yields:

$$X_M = \frac{1/2\sqrt{\sigma_1^2 - \sigma_1\sigma_2 - \sigma_1\sigma_3 + \sigma_2\sigma_3}\cdot\sin\psi\cdot(\sigma_2 - \sigma_3)\cdot(\cos\theta - 1)}{2\sigma_1 - \sigma_2 - \sigma_3 - (\sigma_2 - \sigma_3)\cdot\cos\theta\cdot\cos\psi}$$

$$Y_M = \frac{(\sigma_2 - \sigma_3)\cdot[\sigma_2 - \sigma_3 - (2\sigma_1 - \sigma_2 - \sigma_3)\cdot\cos\theta\cdot\cos\psi] + (\sigma_1^2 - \sigma_1\sigma_2 - \sigma_1\sigma_3 + \sigma_2\sigma_3)\cdot\cos\theta}{2\sigma_1 - \sigma_2 - \sigma_3 - (\sigma_2 - \sigma_3)\cdot\cos\theta\cdot\cos\psi} + \frac{2\sigma_1 + \sigma_2 + \sigma_3}{4}$$

$$Z_M = \frac{1/2\sqrt{\sigma_1^2 - \sigma_1\sigma_2 - \sigma_1\sigma_3 + \sigma_2\sigma_3}\cdot\sin\theta\cdot[2\sigma_1 - \sigma_2 - \sigma_3 - (\sigma_2 - \sigma_3)\cdot\cos\psi]}{2\sigma_1 - \sigma_2 - \sigma_3 - (\sigma_2 - \sigma_3)\cdot\cos\theta\cdot\cos\psi} \tag{8}$$

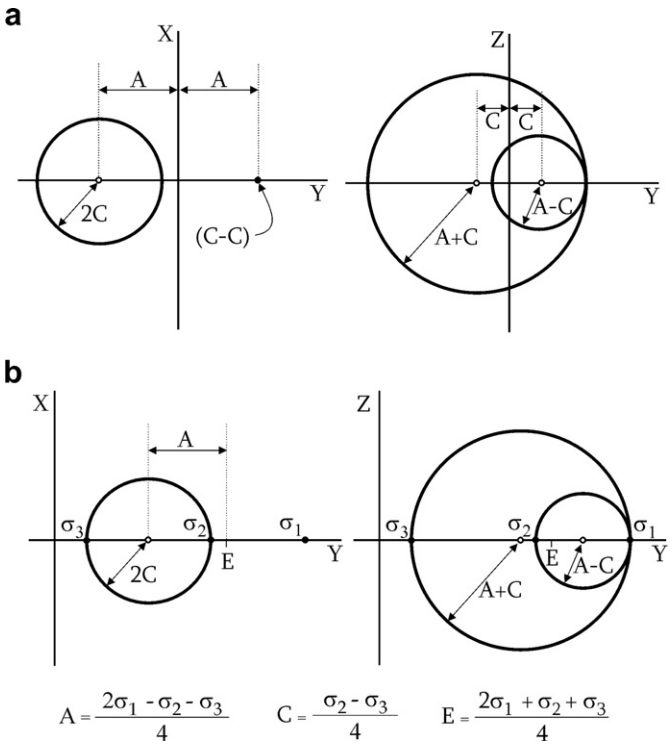

Fig. 5. (a) Parameters used to define a general single-crescent cyclide with $C = D$ (compare with Fig. 2). (b) The same parameters adapted to define a Mohr-cyclide for stress. Note that E shifts the Mohr-cyclide from the origin.

A similar substitution can be done for Eq. (1), but Eqs. (8), although lengthy, are not complex and are definitely more practical to compute because they require only simple trigonometry, without involving 4th-degree polynomials.

A Mohr-cyclide for stress can, thus, be constructed using either:

(1) The magnitudes of stress of a population of planes, with angles φ ($\sigma \wedge \sigma_n$) and δ ($N_S \wedge \sigma_1$) and Eq. (5); or
(2) The principal stress values and Eqs. (8).

2.3. Alternative Mohr-cyclides for stress

Mohr-cyclides for stress are, as seen above, simple-crescent cyclides with a converging point at the principal maximum stress. Although σ_1 was chosen as the most useful reference axis (Fig. 6a), it is possible to define δ with respect to any of the other principal stresses, which results in a change of the cyclide's converging point. Doing this, even for the same relative magnitude of principal stresses, produces dramatic geometric differences.

Using σ_3 as reference axis, the Mohr-cyclide keeps its simple-crescent shape, although reversed with respect to σ_1-cyclides (Fig. 6c), because the convergence point is the minimum principal stress. Accordingly, $\sigma_1\sigma_2$ is now horizontal, producing a "bulkier" shape, while $\sigma_1\sigma_3$ and $\sigma_2\sigma_3$ are vertical in Mohr-space. The greatest geometric change appears when the intermediate σ_2 is chosen as reference axis: the Mohr-cyclide loses the simple-crescent shape and becomes a torus with a converging point at σ_2 (Fig. 6b). The difference in surface shape is part of a continuous transition in the cyclide family, which results from "sliding" the converging point from the maximum principal stress to the intermediate and minimum values. If one would abandon the condition $\sigma_1 > \sigma_2 > \sigma_3$, and decrease σ_1 gradually in Fig. 6, the crescent would change to a sphere ($\sigma_1 = \sigma_2$), then a torus ($\sigma_2 > \sigma_1 > \sigma_3$), a second sphere ($\sigma_1 = \sigma_3$) and finally a reversed crescent cyclide ($\sigma_2 > \sigma_3 > \sigma_1$). The three possible cyclides are defined by the same stress tensor and can be interpreted as equivalent Mohr-diagrams. The significance of the reference axes, however, changes with the principal stress reference axis selected for each case. Note that, despite the geometrical disparity resulting from different references, all these three geometries are reduced to the same two-dimensional Mohr-circles diagram (inbox in Fig. 6).

2.4. Interpretation

2.4.1. Normal and shear stress

The departure from 2D Mohr representations with Cartesian axes labelled σ_n and τ implies that coordinates in Mohr-cyclides must be interpreted differently. While σ_n can still be read directly as the Y-Mohr coordinate (Y_M), there is no similar parallel for the value of τ, which is now a vector in the X_MY_M plane. The Cartesian coordinates of this 3D representation should be read as follows (Figs. 4b and 6):

(1) X_M: $\tau_{(\sigma 1)}$, component of τ in the σ_1 direction
(2) Y_M: σ_n, normal stress (as in 2D)
(3) Z_M: $\tau_{(\perp \sigma 1)}$, component of τ in the plane orthogonal to σ_1

If the cyclide is defined with respect to a principal stresses other than σ_1, then this interpretation must be changed accordingly as illustrated in Fig. 6.

2.4.2. Angles with principal stresses

Mohr diagrams are especially useful because they allow quantification of the angles between the pole to a plane, N_P, and the principal stresses, σ_1, σ_2 and σ_3. In Mohr-circles, angles α, β and γ, can be read in two ways (Fig. 3): directly, considering lines parallel to τ at σ_1, σ_2 and σ_3, or as double angles in the principal planes of stress, $\sigma_1\sigma_2$, $\sigma_1\sigma_3$ and $\sigma_2\sigma_3$. Since Mohr-circles are a 2D representation, the angles are all contained in the XY-plane ($\sigma_n\tau$). Equal-angle lines will be represented as arcs in the Mohr-circle plane, in the space limited by the three principal circles (grey area in Fig. 3). These arcs are concentric with respect to the centres of principal circles (dashed lines in Fig. 3). Each angle measures 90° in the plane that does not contain its reference principal stress: α ($P \wedge \sigma_1$) is 90° in $\sigma_2\sigma_3$, β ($P \wedge \sigma_2$) in $\sigma_1\sigma_3$ and γ ($P \wedge \sigma_3$) in $\sigma_1\sigma_2$.

The same principles apply to 3D Mohr-cyclides, though the extra dimension adds insight into how these angles are distributed in space. As before, α, β and γ can be read as single or double angles, but in Mohr-cyclides equal-angle lines are not

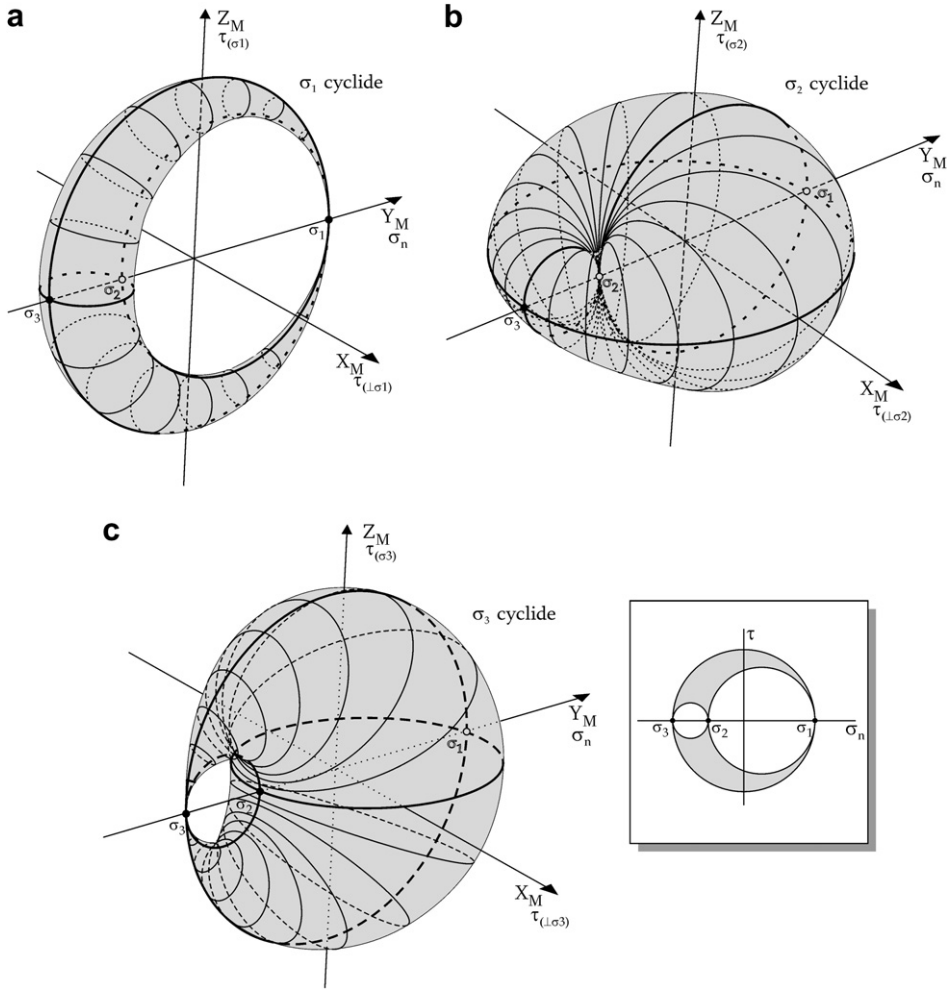

Fig. 6. The three possible Mohr-cyclides for a set of principal stresses: $\sigma_1 = 2$; $\sigma_2 = -1$; $\sigma_3 = -2$. (a) With respect to σ_1; (b) with respect to σ_2; (c) with respect to σ_3. Inbox: the typical Mohr-circle diagram for the same stress values. X_M, Y_M and Z_M are X,Y,Z coordinates in Mohr-space.

confined to a plane and have more complex geometries than concentric arcs (Fig. 7). Only equal-α lines, although not arcs of circles, have a relatively simple geometry. This is because the Mohr-cyclide in Fig. 7 is defined with respect to σ_1.

2.4.3. Geometric variation

Mohr-cyclides for stress are defined by the values of the eigenvectors of $\mathbf{S_{ij}}$, which translate in the physical world as the principal stresses in a particular stress field. Because principal stresses define the stress ellipsoid, Mohr-cyclides are powerful tools to represent graphically its shape variations and the stress state they represent. A compact way to illustrate the relationship between stress ellipsoid and Mohr-cyclide is by means of the stress diagram suggested by Lisle (1979). The graph makes use of the stress ratio,

$$R = \frac{d_1}{d_2} = \frac{\sigma_2 - \sigma_3}{\sigma_1 - \sigma_2} \tag{9}$$

by plotting d_1 values as ordinates and d_2 as abscissas. Other stress ratios could have been used, such as the φ proposed by Angelier (1979) and Etchecopar et al. (1981), or the Lode parameter, to build alternative graphs, but R proves to be the most useful for the present purpose. Fig. 8 illustrates all possible shapes of Mohr-cyclides, defined with respect to σ_1, and allows the following observations:

(a) *Oblate stress ellipsoids*, characterised by $\sigma_1 = \sigma_2 > \sigma_3$, $R = \infty$ and typical of axial extension stress states, plot in the d_1-axis and are represented by *spheres*. This applies to both uni- and biaxial extensions.

(b) On the other hand, the (uni- or bi-) axial compression represented by *prolate stress ellipsoids*, with $\sigma_1 > \sigma_2 = \sigma_3$ and $R = 0$, plots in the d_2-axis. The Mohr-cyclide for this state is a *circle*.

(c) Hydrostatic stress, where $\sigma_1 = \sigma_2 = \sigma_3$, is given by a point at the origin of the diagram. In Mohr-space, hydrostatic stress is also represented by a point.

(d) Intermediate situations, with $\sigma_1 \neq \sigma_2 \neq \sigma_3$, are given by Mohr-cyclides (in this case single-crescent cyclides) with different proportions, according to their R-value.

(e) The fact that some stress ellipsoids can be represented in Mohr-space by spheres and circles is in no contradiction with the statement that three-dimensional Mohr-diagrams are surfaces of the cyclide family. Spheres can be interpreted as

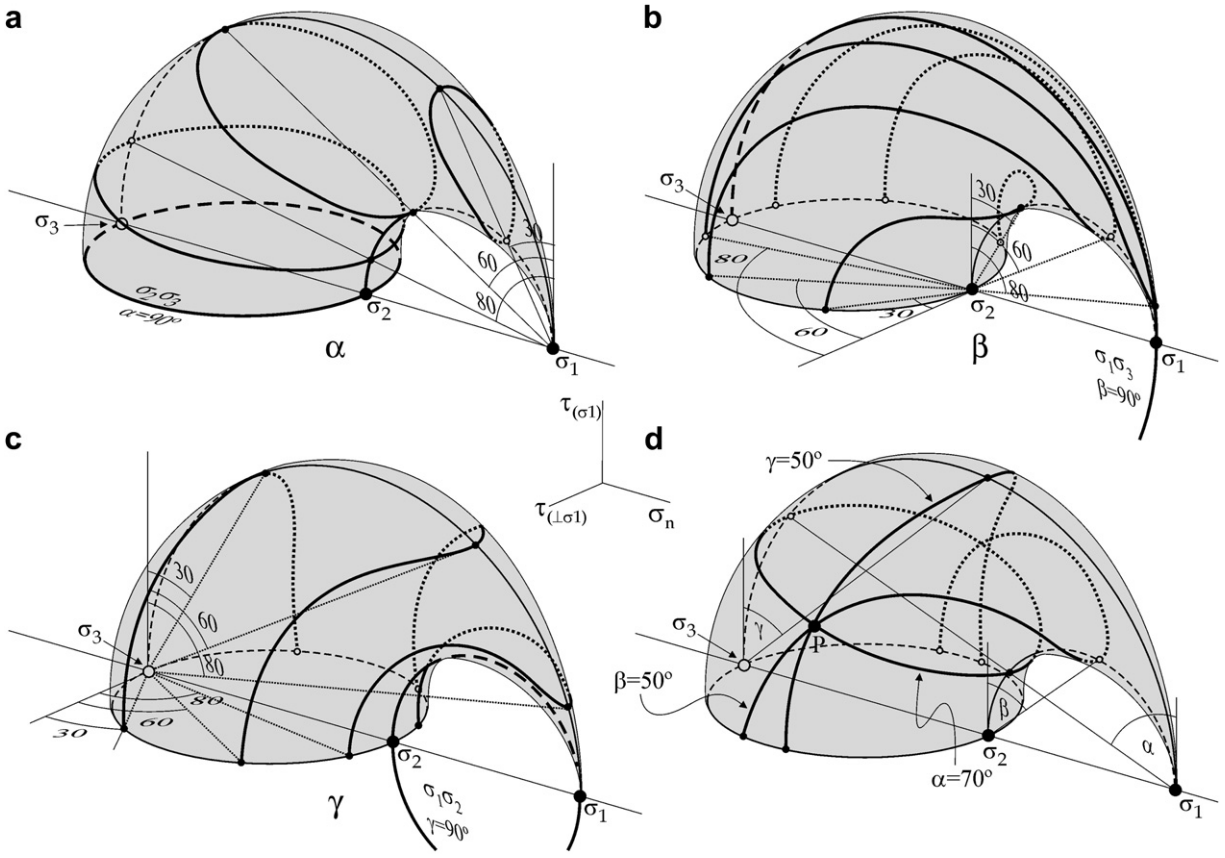

Fig. 7. Equal-angle lines in Mohr-cyclides, considering examples with 30, 60, 80 and 90°: (a) α, (b) β and (c) γ; (d) Example with $\alpha = 70°$, $\beta = 50°$ and $\gamma = 50°$ (P of Figs. 3 and 4). Mohr-cyclides are symmetric with respect to the $\tau_{(\perp\sigma 1)} - \sigma_n$ plane.

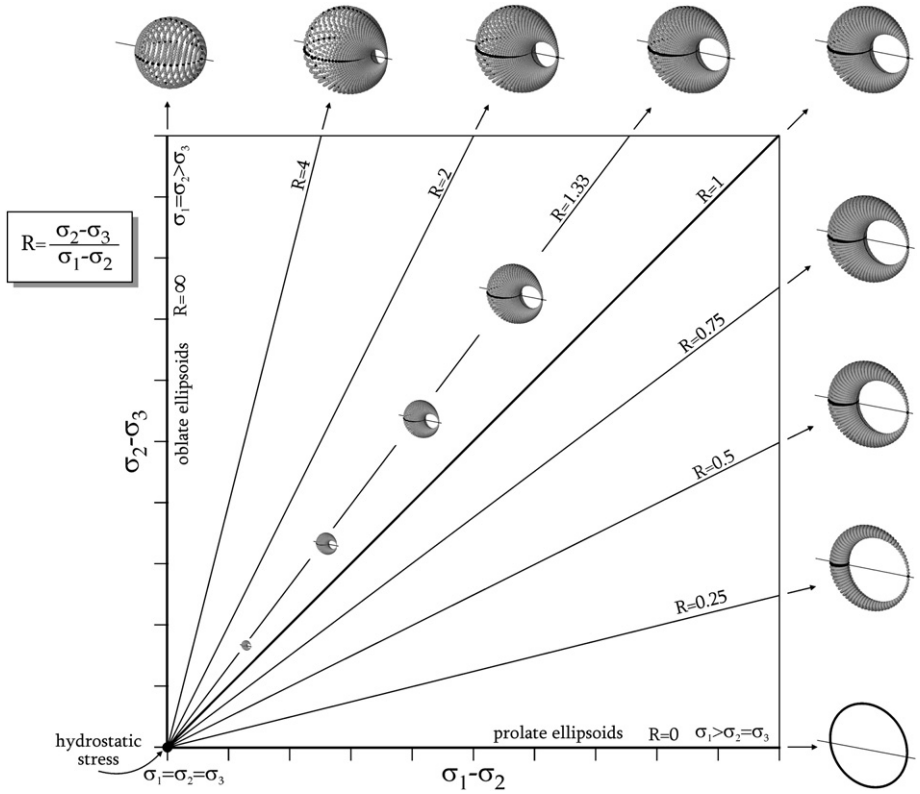

Fig. 8. Different shapes of Mohr-cyclides for stress, illustrated in the diagram proposed by Lisle (1979), according to variation of the stress ratio R.

a special type of cyclide, the surface that forms the transition between single crescent cyclides and torii. Although simpler analytical solutions are the norm in common use, spheres can also be described with the implicit or parametric equations of the cyclide family (Eqs. (1) and (2)). The same reasoning applies to circles.

3. Mohr-cyclides for flow

3.1. The flow tensor

The flow tensor, known also as the velocity gradient tensor ($\mathbf{L_{ij}}$), describes the velocity field of any point in a homogeneously deforming body (e.g. Spencer, 1980):

$$L_{ij} = \frac{\partial v_i}{\partial x_j} \quad v_i = L_{ij} x_j \tag{10}$$

The flow tensor can be decomposed into its symmetric ($\mathbf{D_{ij}}$) and antisymmetric ($\mathbf{W_{ij}}$) components (e.g. Spencer, 1980; Lister and Williams, 1983; Means, 1983). The partitioning of $\mathbf{L_{ij}}$ is additive:

$$L_{ij} = D_{ij} + W_{ij} \tag{11}$$

$\mathbf{D_{ij}}$ is a symmetric quantity and its eigenvectors are known as the *instantaneous stretching axes* of flow (ISA_i). The eigenvalues associated with these directions are the *instantaneous stretching rates*, $\dot{s}_i$ (e.g. Lister and Williams, 1983; Means, 1983).

$\mathbf{W_{ij}}$, the antisymmetric or skewed part, is the vorticity tensor and represents the rotational component of flow and the angular velocities (ω) of lines. The w_i components of $\vec{w}$, the vorticity vector defined with respect to the ISA, can be read directly from the vorticity tensor $\mathbf{W_{ij}}$ (Means et al., 1980):

$$W_{ij} = \begin{vmatrix} 0 & -1/2w_z & 1/2w_y \\ 1/2w_z & 0 & -1/2w_x \\ -1/2w_y & 1/2w_x & 0 \end{vmatrix} \tag{12}$$

The magnitude of $\vec{w}$, $\overline{w}$, and the stretching rates along the ISA may vary by some orders of magnitude. The problem is solved by defining a normalising parameter $\overline{s}$, the mean stretching rate in the section normal to vorticity in monoclinic flows (Passchier, 1997):

$$\overline{s} = \frac{\left|\dot{s}_j - \dot{s}_k\right|}{2} \tag{13}$$

Dividing $\overline{w}/2$ by $\overline{s}$ we obtain the *sectional kinematic vorticity number*:

$$W_K = \frac{\overline{w}}{\left|\dot{s}_j - \dot{s}_k\right|} \tag{14}$$

W_K is intimately connected with the nature of $\mathbf{L_{ij}}$ and can also be defined with the angle between the flow apophyses at *jk* (Bobyarchick 1986; Passchier, 1987):

$$W_{K_i} = \cos\left(e_j \wedge e_k\right) = \cos \upsilon \tag{15}$$

Passchier (1997, 1998) derived other kinematic numbers that can be used to further describe monoclinic flows, namely the *sectional kinematic dilatancy number*, A_K, which defines the rate of area change in the jk-plane, and the *sectional kinematic extrusion number*, T_K, a measure of the stretching rate along the vorticity direction. W_K, A_K, and T_K are dimensionless numbers that fully describe the geometry of a flow with vorticity parallel to ISA_i (e_i) and normal to the plane ISA_jISA_k (e_je_k) (Passchier, 1997).

3.2. Mohr-circles for monoclinic flow

Mohr-circles for the flow tensor $\mathbf{L_{ij}}$, first introduced by Lister and Williams (1983, following Platt), have the following properties (Fig. 9):

(1) The coordinate axes X_M,Y_M represent, respectively, $\dot{s}$—stretching rate and $\dot{\omega}$—rate of angular velocity.
(2) As for stress, the Mohr-circle is defined by the diameter L_{11};$-L_{21}$, L_{22};L_{12} (cf. Means, 1982).
(3) The maximum and minimum stretching rates plot in the diameter parallel to the $\dot{s}$-axis; they represent the maximum and minimum instantaneous stretching axes: ISA_1 and ISA_2.
(4) Any point m, with $\eta = m \wedge ISA_1$ measured counter clockwise in real and Mohr space, has $\dot{\omega}_m$ angular velocity and $\dot{s}_m$ stretching rate.
(5) The Mohr-circle intersects the abscissa at e_1 and e_2, the two single directions of no angular velocity—the eigenvectors of $\mathbf{L_{ij}}$; $\upsilon = e_1 \wedge e_2$. Some flows have only one eigenvector and others none; in these cases, the Mohr-circle has one or zero intersections with the abscissa.

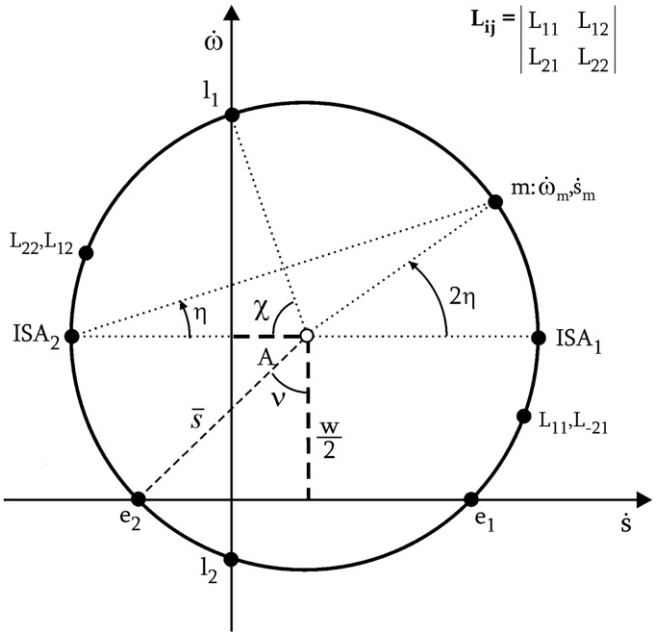

Fig. 9. Mohr-circle for the velocity gradient tensor, $\mathbf{L_{ij}}$.

(6) The Mohr-circle intersects the ordinate at $\mathbf{l_1}$ and $\mathbf{l_2}$, the two single directions of no instantaneous stretch; $\chi = \mathbf{l_1} \wedge \mathbf{l_2}$. As in (5), it is possible to have only one or zero intersections with the ordinate.
(7) From (3) it is clear that the radius of the Mohr-circle corresponds to the mean stretching rate $\bar{s}$: $(ISA_1 - ISA_2)/2$.
(8) Coordinates of the Mohr-circle centre are of special significance: the ordinate of the centre is half the magnitude of the vorticity vector—$w/2$ (cf. 5); the abscissa A is a measure of area change, closely related to A_K:

$$A_K = \cos\chi$$

$$A = A_K \cdot \bar{s} \tag{16}$$

Mohr-circles are, thus, able to represent different types of two-dimensional flow, such as pure shear, general non-coaxial or special types of pulsating flows. The relationship between Mohr-circle geometry and the characteristics of $\mathbf{L_{ij}}$, allows the diagrams to be useful as a gauge of flow parameters (Passchier and Urai, 1988; Passchier, 1990b; 1991) or as elements to study inhomogeneous progressive deformation (Means, 1983).

3.3. Plotting procedure

The procedure followed in this section is in some ways analogous to the description of stress-cyclides, although adapted to the characteristics of a flow tensor. The most important divergence is that, unlike $\mathbf{S_{ij}}$, the flow tensor does not have to be symmetric. The degree of symmetry of flow depends on the relationship between the vorticity vector and the ISA: if $\vec{w}$ is parallel to one of the ISA, flow is considered monoclinic; if not, the flow has triclinic geometry (e.g. Robin and Cruden, 1994; Jiang and Williams, 1998; Iacopini et al., 2007).

We define the flow tensor as, following the additive properties of $\mathbf{L_{ij}}$ (Means et al., 1980):

$$L_{ij} = \begin{vmatrix} \dot{s}_x & -w_z/2 & 0 \\ w_z/2 & \dot{s}_y & 0 \\ 0 & 0 & \dot{s}_z \end{vmatrix} \tag{17}$$

The main advantage of this notation is that principal stretches and components of $\vec{w}$ are given directly from tensor components. $\mathbf{L_{ij}}$ describes the velocity field of an imaginary particle at a point m in space, defined by the position vector $\vec{m}$ (Fig. 10a):

$$\vec{v}_i = L_{ij}\vec{m}_j \tag{18}$$

This operation results in three velocity vectors, oriented with respect to the reference axis; using tensor notation of Eq. (17), these are coincident with the ISA and $\vec{w}$ will be parallel to one of them. These velocity vectors define $\dot{d}$, the rate of displacement vector, also a velocity; its magnitude, $\bar{d}$, is given by:

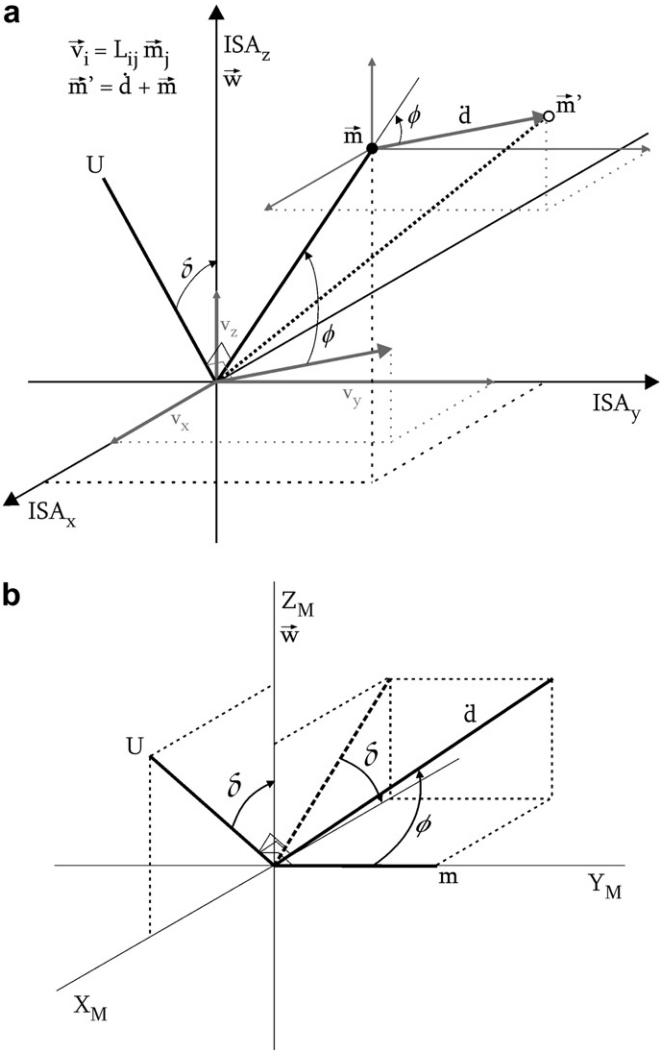

Fig. 10. Two representations of the effect of flow tensor on the position vector m: (a) in real space; (b) in Mohr space.

$$\bar{d} = \sqrt{v_x^2 + v_y^2 + v_z^2} \tag{19}$$

The orientation of $\dot{d}$ in space is crucial to build Mohr-cyclides for flow and is given by two angles, φ and δ (Fig. 14a). φ is the angle between $\dot{d}$ and $\vec{m}$, given by the dot-product:

$$\cos\varphi = \frac{m_x v_x + m_y v_y + m_z v_z}{d} \tag{20}$$

δ is the angle between U, the pole of the plane defined by $\dot{d}$ and $\vec{m}$, and one of the eigenvectors of $\mathbf{L_{ij}}$. Since the Mohr-cyclide is being constructed for monoclinic flow, it is useful to choose the eigenvector that lies parallel to the vorticity vector $\vec{w}$, and thus, δ can be defined simply as $U \wedge \vec{w}$:

$$\cos\delta = \frac{U_x w_x + U_y w_y + U_z w_z}{\bar{U} \cdot w} \tag{21}$$

U_i components are obtained with the cross-product of $\vec{m}$ and $\dot{d}$. With vorticity fixed in the zz-axis in Mohr-space,

irrespective of its real orientation in real space, the Mohr-cyclide can now be plotted with the following polar coordinates (Fig. 10b):

$$X_M = \overline{d}\cdot\sin\varphi\cdot\cos\delta$$

$$Y_M = \overline{d}\cdot\cos\varphi$$

$$Z_M = \overline{d}\cdot\sin\varphi\cdot\sin\delta \tag{22}$$

Alternatively, Mohr-cyclides for monoclinic flows can be described by the general cyclide equations (Eqs. (1) and (2)), adapted to reflect the geometry of a flow tensor as done above for stress. There are, however, two major differences. First, $\mathbf{L_{ij}}$ does not have to be symmetric, in fact it is not for all non-coaxial flows. Second, angle δ in flow-cyclides is measured with respect to $\overrightarrow{w}$ (which can be parallel to any of the ISA), whereas in stress, δ is tagged to σ_1. Considering the general case where the vorticity vector $\overrightarrow{w}$ is parallel to the i-axis and ISA$_i$, parameters A, C and E can be redefined with the formulas (Fig. 11):

$$A = \sqrt{\left(E_y - \dot{s}_i\right)^2 + E_x^2}$$

$$C = \frac{\left|\dot{s}_j - \dot{s}_k\right|}{4}$$

$$E = \begin{cases} E_x = \frac{w_i}{4} \\ E_y = \frac{2\dot{s}_i + \dot{s}_j + \dot{s}_k}{4} \end{cases} \tag{23}$$

As before, $B^2 = A^2 - C^2$ and D is equal to C or A. Fig. 11 illustrates the case where $\overrightarrow{w}$ is parallel to zz, i.e., when $\overrightarrow{w}$ has only w_z components (Eq. (17)), but the construction will be similar in all aspects for the other two orientations of $\overrightarrow{w}$. Table 1 summarises the parameters for all scenarios. Mohr coordinates for any point (θ,ψ) will be obtained by substituting these parameters in Eq. (2). This procedure produces a set of coordinates that define a cyclide with appropriate shape and parameters, but symmetric with respect to the Y_MZ_M- and X_MY_M-planes. Because flow may have an asymmetric component, it is necessary to define an angle to rotate the parametric cyclides, in order to assure geometrical correspondence with their tensor. This step can be accomplished with a general rotation tensor $\mathbf{R_{ij}}$ with a rotation vector normal to Z_M (because symmetry in the X_MY_M-plane is desirable following the convention for δ). The rotation angle ρ is the angle between the negative Y_M and the cyclide vertical symmetry plane. ρ is defined by the expressions:

$$\rho = \arctan\left(\frac{w_i}{2\dot{s}_1 - \dot{s}_2 - \dot{s}_3}\right) \quad if \quad \dot{s}_i > E_y,$$

or

$$\rho = 180^\circ - \arctan\left(\frac{w_i}{2\dot{s}_1 - \dot{s}_2 - \dot{s}_3}\right) \quad if \quad \dot{s}_i < E_y \tag{24}$$

which, since they are equivalent to:

$$\tan\rho = \frac{W_K}{A_K - 2T_K}, \tag{25}$$

characterise ρ as a gauge for non-coaxiality of the flow: for $\rho = 0^\circ$, W_K is zero, the flow is coaxial and the cyclide is symmetric in the Y_MZ_M-plane. By convention, ρ is measured counter-clockwise for flows with $W_K > 0$ and clockwise if $W_K < 0$. The rotated coordinates of the parametric Mohr-cyclide can now be obtained by simple multiplication of X_M°, Y_M°, Z_M° by $\mathbf{R_{ij}}$:

$$X_M = X_M^\circ\cdot\cos\rho - Y_M^\circ\cdot\sin\rho + E_x$$

$$Y_M = X_M^\circ\cdot\sin\rho + Y_M^\circ\cdot\cos\rho + E_y$$

$$Z_M = Z_M^\circ \tag{26}$$

Again, the components of parameter E must be added to remove the cyclide centre from the origin.

The third method to draw Mohr-cyclides gives an outline of their shape and uses the tensor components directly, in a way similar to the plotting scheme proposed by Means (1982) (Fig. 12). The construction for a flow tensor with $\dot{s}_x < \dot{s}_y < \dot{s}_z$ and ISA$_1$ parallel to $\overrightarrow{w}$ and e_1 at zz-axis, proceeds as follows:

(1) $\mathbf{L_{ij}}$'s reference axes (the ISA, Eq. (17)) are plotted in Mohr-space with coordinates:
ISA$_1$: $\{0, \dot{s}_1, 0\}$ (component reversal)
ISA$_2$: $\{w_z/2, \dot{s}_2, 0\}$ (sign change)
ISA$_3$: $\{w_z/2, \dot{s}_3, 0\}$ (component reversal; Fig. 12a)
(2) ISA$_2$ and ISA$_3$ (in this example) define a diameter of a circle, parallel to Y_M. This circle intersects Y_M at e_2 and e_3, two eigenvectors of $\mathbf{L_{ij}}$. The line connecting the centre of the circle and $\dot{s}_1$ intersects the circle at points q and r (Fig. 12b).
(3) Line segments ISA$_1$-r and ISA$_1$-q define the diameters of two additional vertical circles. These three circles are the three major circles of a single crescent cyclide (Fig. 12c) or a torus, in the case of ISA$_2$ parallel to $\overrightarrow{w}$.

Summarising, Mohr-cyclides for monoclinic flow can be:

(1) Accurately plotted using polar coordinates (Eq. (22); Fig. 10);
(2) Accurately plotted using parametric equations (Eq. (26); Table 1; Fig. 11);
(3) Outlined from the tensor components (Fig. 12).

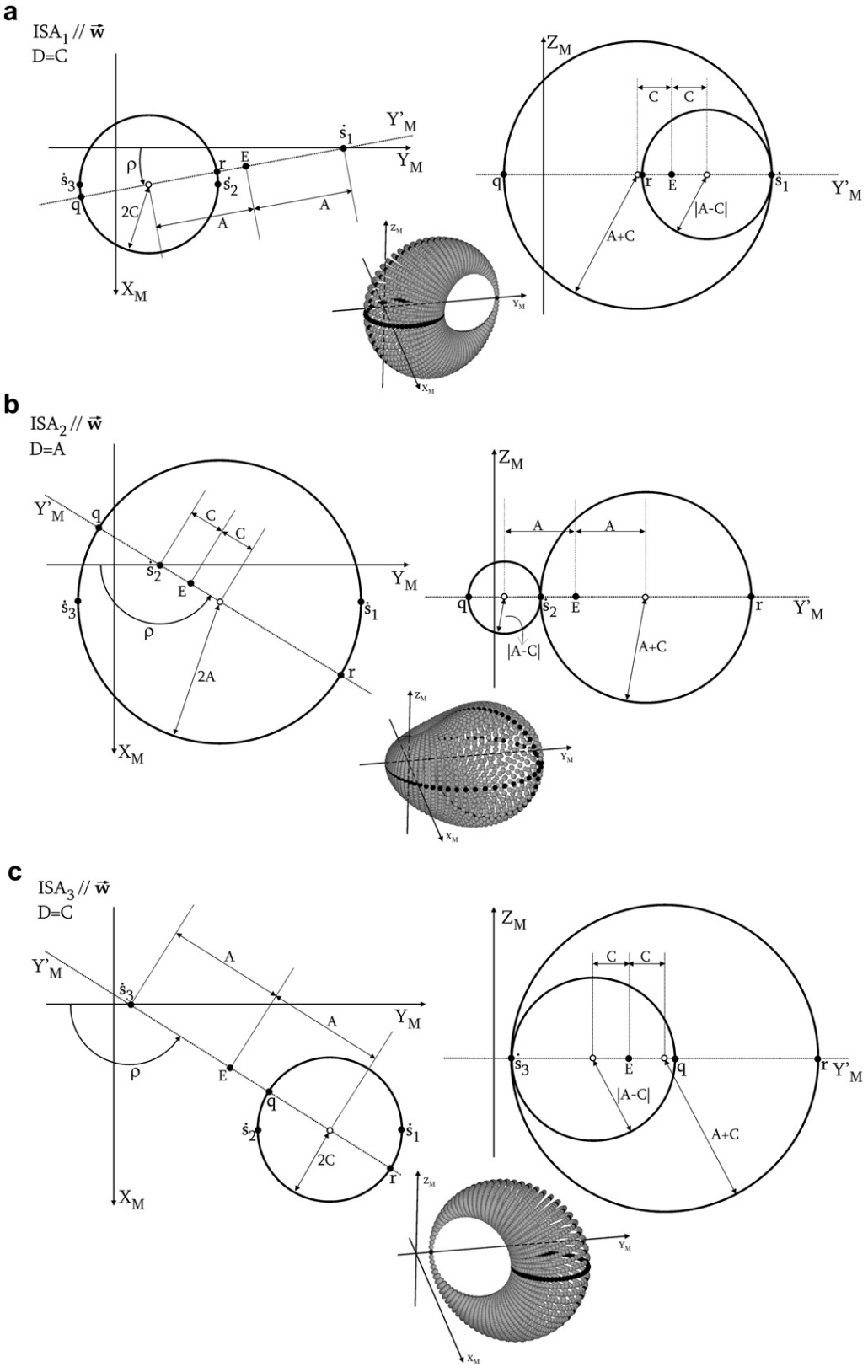

Fig. 11. The cyclide parameters for the three possible orientations of the vorticity vector in the reference frame: (a) parallel to ISA_1; (b) to ISA_2 and (c) to ISA_3.

Table 1
Parameters for flow Mohr-cyclides

ISA $_z$	Cyclide shape	Cyclide parameters (vorticity parallel to z – Eq.17; Fig.11)				
		A	***C***	***D***	***Ex***	***Ey***
ISA$_1$ / **ISA$_3$**	Single-crescent	$\sqrt{(E_y - s_z)^2 + E_x^2}$	$\frac{\lvert s_x - s_y \rvert}{4}$	*C*	$\frac{w_z}{4}$	$\frac{s_x + s_y + 2s_z}{4}$
ISA$_2$	Torus	$\frac{\lvert s_x - s_y \rvert}{4}$	$\sqrt{(E_y - s_z)^2 + E_x^2}$	*A*		
ISA$_y$	**Cyclide shape**	**Cyclide parameters (vorticity parallel to y)**				
		A	***C***	***D***	***Ex***	***Ey***
ISA$_1$ / **ISA$_3$**	Single-crescent	$\sqrt{(E_y - s_y)^2 + E_x^2}$	$\frac{\lvert s_x - s_z \rvert}{4}$	*C*	$\frac{w_y}{4}$	$\frac{s_x + 2s_y + s_z}{4}$
ISA$_2$	Torus	$\frac{\lvert s_x - s_z \rvert}{4}$	$\sqrt{(E_y - s_y)^2 + E_x^2}$	*A*		
ISA$_x$	**Cyclide shape**	**Cyclide parameters (vorticity parallel to x – Eq.27)**				
		A	***C***	***D***	***Ex***	***Ey***
ISA$_1$ / **ISA$_3$**	Single-crescent	$\sqrt{(E_y - s_x)^2 + E_x^2}$	$\frac{\lvert s_y - s_z \rvert}{4}$	*C*	$\frac{w_x}{4}$	$\frac{2s_x + s_y + s_z}{4}$
ISA$_2$	Torus	$\frac{\lvert s_y - s_z \rvert}{4}$	$\sqrt{(E_y - s_x)^2 + E_x^2}$	*A*		

3.4. Interpretation

3.4.1. Reference frame and special sections

In two dimensions (Fig. 9), the abscissa Y_M in Mohr space is labelled $\dot{s}$, the stretching rate, whereas the ordinate X_M stands for $\dot{\omega}$, the rate of angular velocity. Expanding Mohr space to three dimensions creates another reference axis, Z_M. The physical meaning of this extra coordinate is related to the significance of angle δ, defined, as seen above, with respect to $\vec{w}$: Z_M represents a second angular velocity rate, measured parallel to the vorticity vector, and not a second stretching rate. Thus, the coordinates of a point in a Mohr-cyclide for flow represent:

(1) X_M: $\dot{\omega}_{(\perp \mathbf{w})}$, component of the angular velocity rate normal to the vorticity vector;
(2) Y_M: $\dot{s}$, stretching rate (as in 2D);
(3) Z_M: $\dot{\omega}_{(\mathbf{w})}$, component of angular velocity rate parallel to the vorticity vector.

A cyclide is a three-dimensional surface and, as such, can be cut in all directions in space. Some of these cross-sections have special significance when the cyclide is interpreted as a Mohr-diagram for flow. Angle δ defines two of these important sections (Fig. 13):

(1) $\boldsymbol{\delta = 0^\circ}$, $\boldsymbol{\delta = 180^\circ}$ (Fig. 13a) characterises lines where the displacement vector $\dot{d}$ is normal to $\vec{w}$, i.e., particles moving in the plane normal to vorticity, the VPP (the *vorticity profile plane* cf. Robin and Cruden, 1994). Accordingly, in Mohr-space, these particles plot as a circle in the X_MY_M-plane, with $Z_M = 0$ and, therefore, there is no angular velocity component parallel to $\vec{w}$. This circle includes the ISA and the eigenvectors normal to vorticity, as well as $\mathbf{l_1}$ and $\mathbf{l_2}$, the lines of no instantaneous stretch. The $\delta = 0^\circ$ circle is also a symmetry plane of the cyclide and, thus, one of the defining circles of its parametric equations. It is essential to point out that this circle is also the equivalent of 2D Mohr-circles in the Mohr-cyclide (compare with Fig. 9; proof in Section 4), always defined in the VPP. Thus, the coordinates of the centre can also be read as gauges for the W_K and A_K parameters.

(2) $\boldsymbol{\delta = 90^\circ}$ (Fig. 13b) is the geometrical locus of particles with $\dot{d}$ in planes that contain the vorticity vector and one of the $\vec{w}$ normal eigenvectors (the flow apophyses). The eigenvector planes do not have an angular velocity component normal to $\vec{w}$ and $X_M = 0$. Depending on the number of real (non-imaginary) eigenvalues of $\mathbf{L_{ij}}$, there can be 2, 1 or no planes with $\delta = 90^\circ$. In the example of Fig. 13b, there are two of these sections, neither of which is a symmetry plane of the cyclide and, as such, cannot be used to calculate cyclide parameters.

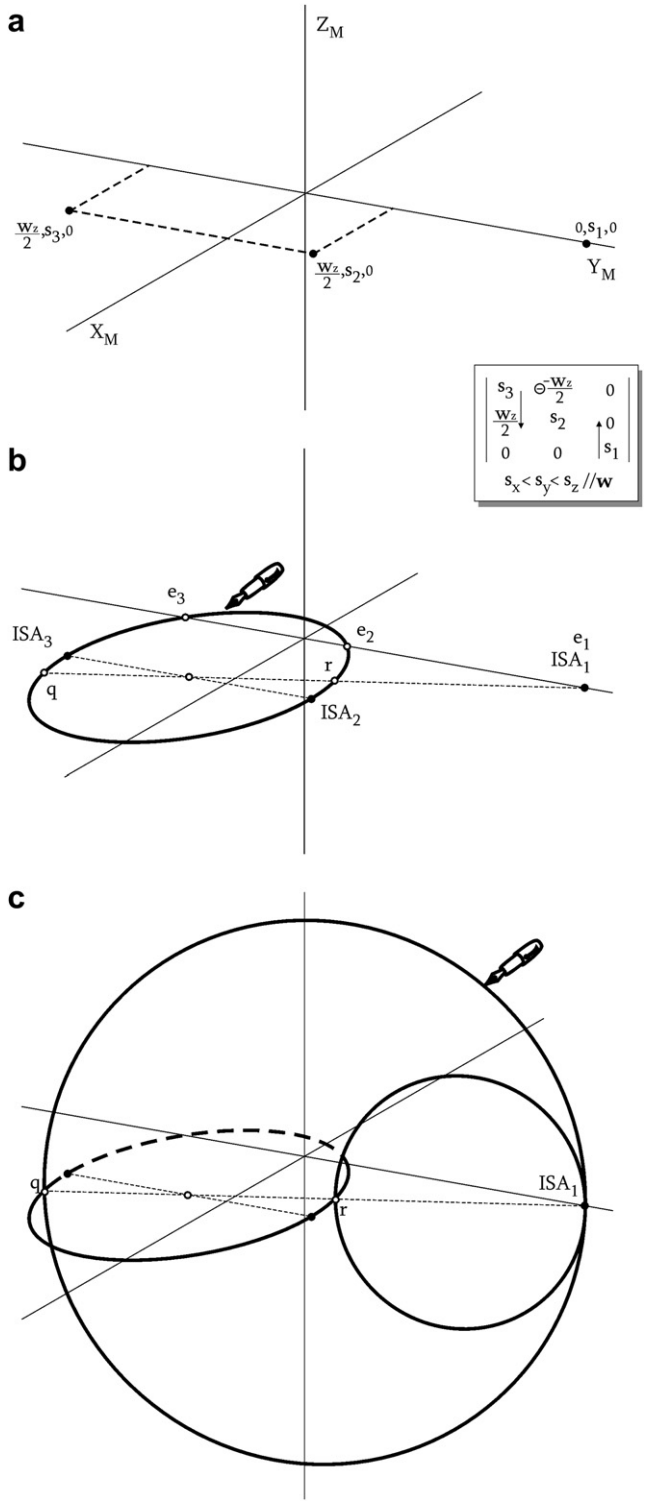

Fig. 12. The three steps to outline the geometry of a Mohr-cyclide from tensor components.

Eigenvector planes are equivalent to cyclide symmetry planes only when the eigenvectors are parallel to the ISA, i.e., in coaxial flow types. The orientation and number of eigenvector planes are important to classify types of flow and estimate particle paths within it: two flow eigenvector occur in general shear (cf. Simpson and De Paor, 1993) with hyperbolic flow paths; one eigenvector plane occurs in simple shear with linear paths; zero eigenvector planes (two imaginary eigenvalues) are present in complex flows with closed and elliptical particle paths (e.g. Ramberg, 1975; Means et al., 1980; Passchier, 1986; Iacopini et al., 2007). In this regard, Mohr-cyclides are useful because they allow an immediate estimation of number eigenvector planes, and therefore, flow type, without referring to eigenvalue calculations. The eigenvector plane sections within the cyclide can be read as Mohr-circles and the orientation of a line k, for instance in the e_2e_3-plane with coordinates $\{0, \dot{\omega}_{//w}, \dot{s}\}$, can be determined with respect to the eigenvectors using the familiar single- or double-angle rule. The eigenvector planes are also important in the sense that one of them is likely to be parallel to the boundaries of a monoclinic shear zone developing in the steady state flow defined by $\mathbf{L_{ij}}$ (Passchier, 1998).

A second set of sections through the cyclide, with geological meaning in terms of monoclinic flow, are the principal sections of the *instantaneous stretching ellipsoid* (Fig. 14). These sections are circles within the cyclide, defined by diameters comprising the ISA coordinates. If flow is coaxial, the sections of the instantaneous stretching ellipsoid are identical to the principal circles of the cyclide. For non-coaxial flow, they are not identical and the diameters of circles ISA_1ISA_3 and ISA_1ISA_2 are related by an angle (ξ in Fig. 14) which only has expression in the Mohr-cyclide. In geographical space, the ISA planes are, by definition, at 90° of each other. The existence of this angle is not conflicting with this statement because, in the Mohr-cyclide, the ISA plot at opposite ends of diameters and, therefore, are orthogonal via the double-angle rule of Mohr-space. Representation of these sections in a typical 2D Mohr-diagram requires more sophisticated construction methods, such as the *locii* of Treagus (1986, 1990), which, although geometrically flawless, are not as intuitive as plain circles.

The special sections of Mohr-cyclides are excellent examples of a useful property of cyclides, which states that all lines in their curvature are circles (Allen and Dutta, 1997; Shene, 2000). From this, it follows that Mohr-cyclides are, in fact, a collection of an infinite number of Mohr-circles defined by their orientations with respect to a reference axis, the vorticity vector, in the case of flow-cyclides. The paradigm of this statement is the cyclide section normal to vorticity (Fig. 13a), the three-dimensional equivalent of the 2D Mohr-circle for flow. This allows Mohr-cyclides the potential to represent, in a simple way, multiple orientations in space, including the vorticity profile plane, the shear zone boundary and odd outcrop surfaces, defined by geomorphological fancy, more often than not in conflict with the structural geologist's convenience.

3.4.2. Geometries and examples of Mohr-cyclides

For monoclinic flow described with Eq. (17), the type of Mohr-cyclide depends first on the relative orientation of the ISA reference frame with respect to the vorticity vector and, second, on the magnitude of the instantaneous stretching axis parallel to it.

Fig. 15 illustrates shape variations of Mohr-cyclides of major flow types, using examples where $\vec{w}$ is parallel to the

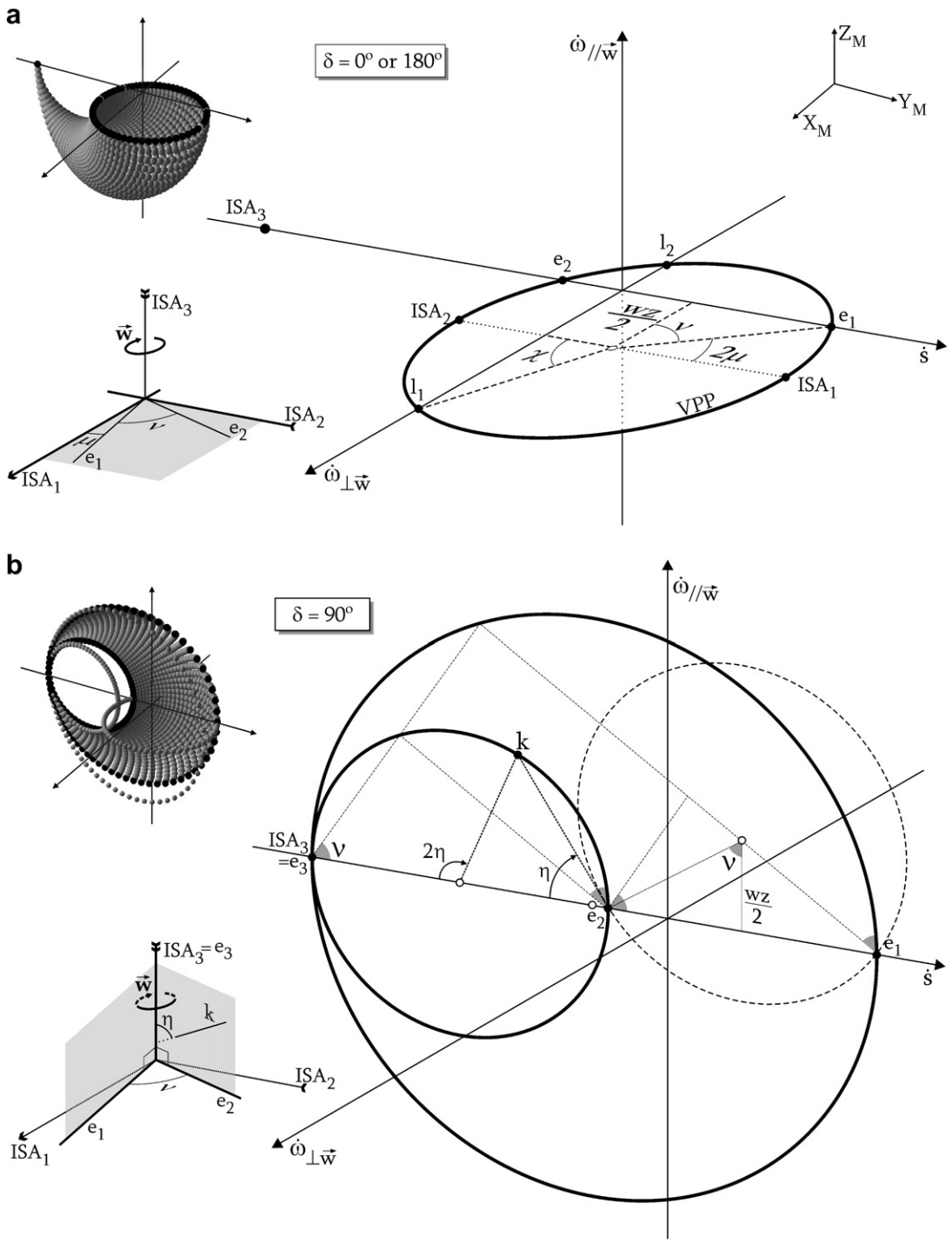

Fig. 13. Sections of the Mohr-cyclide according to angle δ. (a) $\delta = 0/180°$: the VPP, vorticity normal plane; (b) $\delta = 90°$: the "flow planes" (note that the dashed circle is not a part of the cyclide, but the projection of (a) in the *YZ* plane). Small white circles represent the centre of the Mohr-circles within the Mohr-cyclide.

i-axis (Eq. (17)), $\dot{s}_j > \dot{s}_k$ and the value of $\dot{s}_i$ is variable; this is equivalent to a case where flow parameter T_K is allowed to change. Subscripts *i*,*j*,*k* are preferred here because the geometry of Mohr-cyclides depends more on the relative magnitude of principal stretching rates than on their absolute value and is completely independent of their real orientation, as long as the ISA are pinned to a reference frame. Another feature that is important to decide which shape a Mohr-cyclide will assume is the number of eigenvectors of $\mathbf{L_{ij}}$ (e) and their eigenvalues $\dot{e}_i$, compared to the stretching rate parallel to vorticity. Note that the convention $\dot{s}_j > \dot{s}_k$ implies $\dot{e}_j > \dot{e}_k$. For simplicity, this discussion is mainly based on isochoric flows, but the same principles will also apply to situations with volume change.

(a) *Transtensional flow* (Fig. 15a; Sanderson and Marchini, 1984) is characterised by an area increase in the ISA_j–ISA_k plane, compensated by shortening in the direction of $\vec{w}$. In terms of stretching rates, this definition implies $\dot{s}_i < 0$, $\dot{s}_i < \dot{s}_j + \dot{s}_k$ and allows $\dot{s}_i < \dot{s}_k$ as well as $\dot{s}_i > \dot{s}_k$. In isochoric

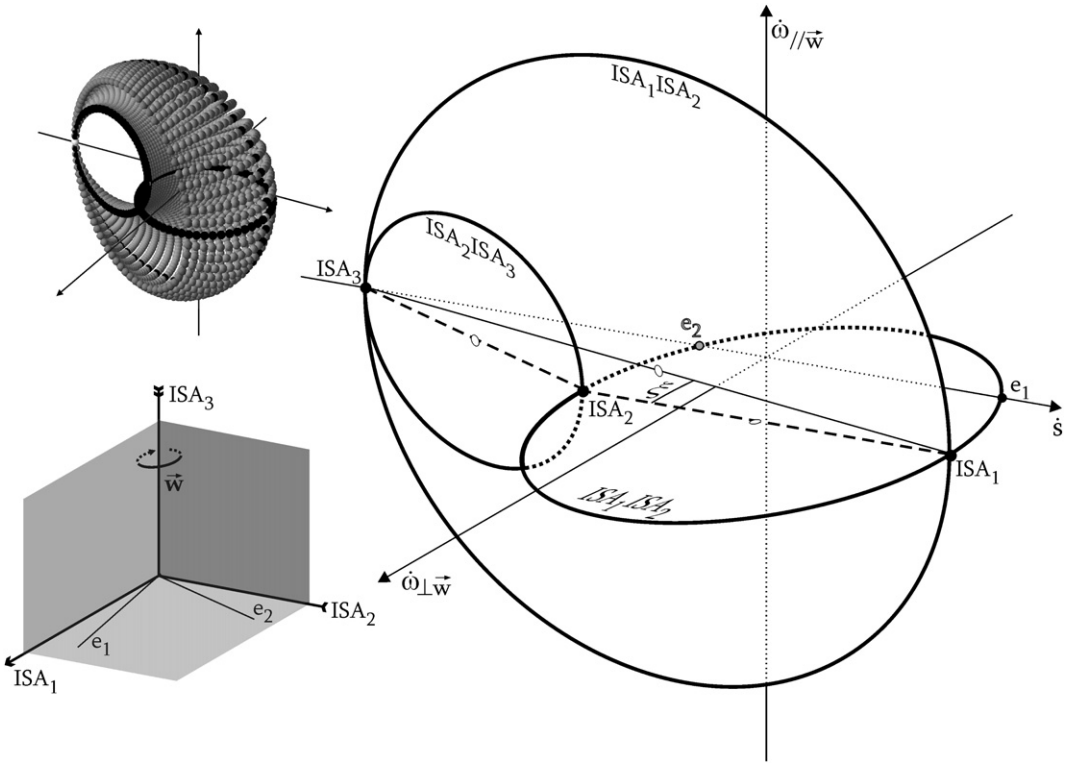

Fig. 14. The three principal planes of the instantaneous stretching ellipsoid.

flow, this means $A_K = -T_K$. Transtension can be represented in Mohr-space by two surfaces of the cyclide family. The transition between the two shapes is governed by the relative magnitude of $\dot{s}_i$ and eigenvalues $\dot{e}_j$, $\dot{e}_k$: if $\dot{s}_i < \dot{e}_j$, $\dot{e}_k$, the Mohr-cyclide will be a *negative crescent cyclide*, a crescent cyclide "facing" the negative end of Y_M; if $\dot{e}_j < \dot{s}_i < \dot{e}_k$, the Mohr-cyclide will be a *torus with a vanishing point* at $\dot{s}_i$ (see Fig. 16 below).

(b) The counterpart of transtension is *transpressional flow* (Fig. 15b; Sanderson and Marchini, 1984), where area decrease on the ISA_j–ISA_k plane is balanced with stretching in the direction of $\vec{w}$. Translating into stretching rate values, the conditions for transpression are $\dot{s}_i > 0$, $\dot{s}_i > \dot{s}_j + \dot{s}_k$, with $\dot{s}_i > \dot{s}_j$ or $\dot{s}_i < \dot{s}_j$. Transpression can be illustrated by *positive crescent* Mohr-cyclides (cyclides "facing" the positive end of Y_M) for $\dot{s}_i > \dot{e}_j$, $\dot{e}_k$ or *torii with a vanishing point* at $\dot{s}_i$ for $\dot{e}_j > \dot{s}_i > \dot{e}_k$(see Fig. 16 below). It is important to note that transpression and transtension are always indistinguishable in 2D Mohr-circles, because these diagrams consider only one section of the bulk flow. Mohr-cyclides include information about stretching rate parallel to vorticity and, thus, allow the differentiation of these two types of flow.

(c) *Simple shear* or *parallel flow* (Fig. 15c) is the simplest form of non-coaxial flows, with no volume change and characterised by a kinematic vorticity number $W_K = 1$ or $W_K = -1$ ($|2w_i| = |\dot{s}_j - \dot{s}_k|$). To ensure laminar flow, $T_K = A_K = 0$, which means that simple shear is always isochoric. Unlike the previous examples, the Mohr-diagram for simple shear flow is neither a cyclide nor a torus, but a *sphere*. This is not in contradiction with the statement that 3D Mohr-diagrams are surfaces from the cyclide family because, as seen above, they represent a continuum in the group and the transition between single crescent cyclides and torii with vanishing points. The sphere touches the $\dot{s}$-axis of the Mohr-diagram only at the origin, which is consistent with the fact that flow tensors for simple shear have only one eigenvector. The eigenvector lies as expected in the plane normal to $\vec{w}$, at 45° with the instantaneous stretching axes. The instantaneous stretching axes are orthogonal, as read, in the form of double-angles, on their respective planes.

Spherical surfaces are not exclusive of simple shear flows (with one eigenvector), as they occur whenever $\dot{s}_i$ equals the stretching rate of one of the eigenvectors in the ISA_j–ISA_k plane. This circumstance, however possible, represents a special case of the Cardano condition, when two of the three real eigenvalues coincide.

(d) *Pure shear*, or coaxial flow, occurs when the eigenvectors of the flow coincide with the instantaneous stretching axes, which translates in $W_K = 0$. Mohr-cyclides for pure shear flow can be represented by different kinds of surfaces, including negative and positive single crescent cyclides, torii, spheres and circles, since the relative magnitudes of $\dot{s}_i$, $\dot{s}_j$ and $\dot{s}_k$ are not relevant. However, they have one thing in common: whatever the shape, the Mohr-cyclide will be symmetric with respect to both the X_MY_M- and the Y_MZ_M-planes and the ISA_jISA_k circle will be centred on the Y_M ($\dot{s}$)-axis. The reason for this is the angular velocity of the instantaneous stretching axes, zero at all times following the definition of coaxial flow, implies that $\dot{\omega}_{(\perp \mathbf{w})} = \dot{\omega}_{(\mathbf{w})} = 0$ (the ISA coordinates X_M and Z_M are always 0).

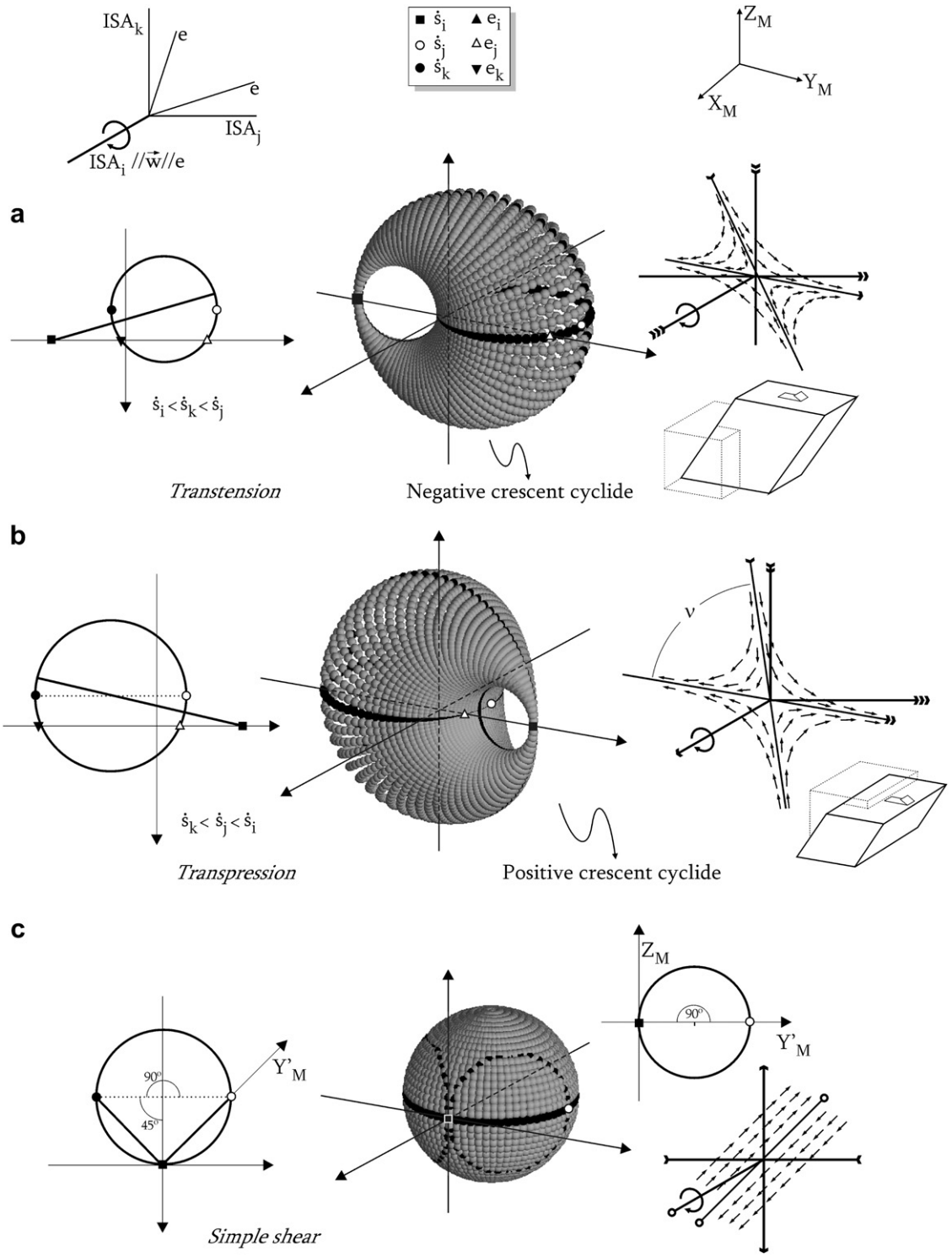

Fig. 15. Some examples of cyclides and their shapes for different types of flow. Each part of the figure shows, from left to right: the basal section of the cyclide (identical to the 2D Mohr circle), the 3D cyclide and an outline of the particle paths (not meant to be accurate). (a) Transtensional flow; (b) transpressional flow; (c) simple shear flow.

(e) *Rotational flow*, or super simple shear (Simpson and De Paor, 1993) occurs whenever the kinematic vorticity number W_K has an absolute value greater than 1. Translating this condition into tensor algebra, it follows that a rotational flow tensor has only one non-imaginary real eigenvalue, in the direction parallel to $\vec{w}$. These special cases produce negative or positive crescent shaped Mohr-cyclides, but never torii surfaces, which require three real eigenvalues. Rotational flows are easily identified by Mohr-cyclides which touch the $\dot{s}$-axis only in one point, at the stretching rate correspondent to the ISA parallel to vorticity.

(f) *Outward-* and *inward-radiant* flow types (Passchier, 1991) are defined by Mohr-cyclides of all shapes, located entirely on the positive or negative $\dot{s}$-axis. Although mathematically possible, the existence of these flow types in Geology is somewhat unrealistic, since they represent either "exploding" or "imploding" flows with extreme volume change. The extreme case of outward- or inward-radiant flows occurs for $A_K = \infty$. On this particular condition, the Mohr-cyclide will be a *circle*. Just as spheres, circles represent a special case of the cyclide family, characterised by $\dot{s}_j = \dot{s}_k$.

The discussion so far can be summarised with an example defined by the tensor (Fig. 16):

$$L_{ij} = \begin{vmatrix} 0.5 & 0 & 0 \\ 0 & -2 & 0.75 \\ 0 & -0.75 & 1.5 \end{vmatrix} \quad \text{in the form}$$

$$L_{ij} = \begin{vmatrix} \dot{s}_x & 0 & 0 \\ 0 & \dot{s}_y & -w_x/2 \\ 0 & w_x/2 & \dot{s}_z \end{vmatrix} \tag{27}$$

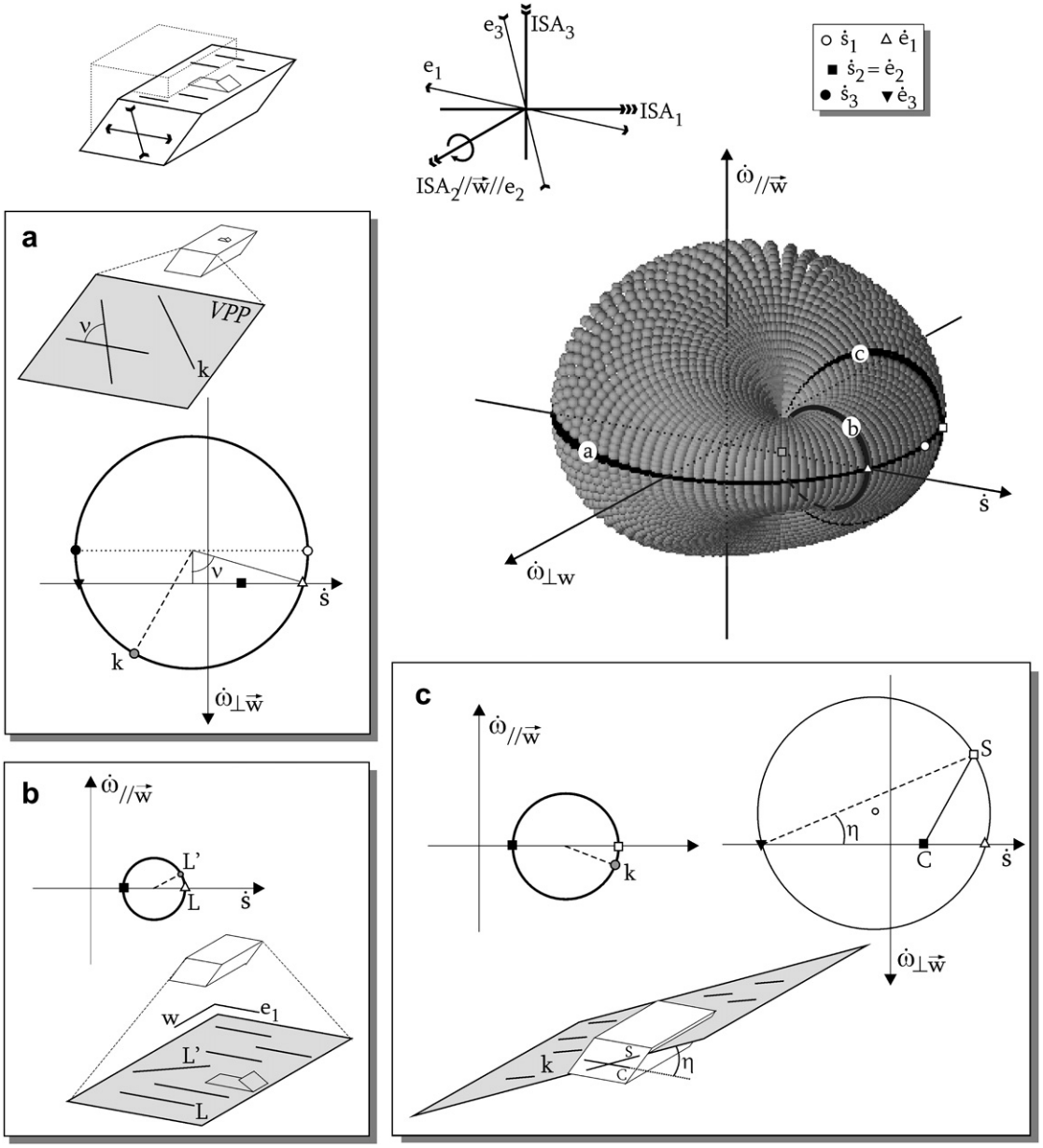

Fig. 16. A Mohr-cyclide for isochoric transpressional flow and three examples of associated Mohr-circles. Discussed in text.

From $\mathbf{L_{ij}}$ components it is possible to deduce that:

(a) $\dot{s}_z < \dot{s}_x < \dot{s}_y$, which means that ISA_1 is parallel to the *yy*-axis in the reference frame, ISA_2 to the *xx*-axis and ISA_3 to the *zz*-axis.
(b) Since $\dot{s}_x = \dot{s}_y + \dot{s}_z$, $T_K = -A_K$, and the flow is isochoric.
(c) The vorticity vector is defined by a negative component and is parallel to ISA_2 at *xx*; shear sense is dextral since $W_K < 0$; the vorticity profile plane (VPP) lies at ISA_1ISA_3.
(d) The relative magnitude of the principal stretching rates suggests that an area decrease in the VPP is compensated by extension in the direction of ISA_2.
(e) (a–d) characterise a *transpressional dextral flow*.
(f) Calculation of the eigenvectors of $\mathbf{L_{ij}}$ shows that the eigenvalue parallel to vorticity is the intermediate ($\dot{e}_2$); from this it follows that an eventual material line attractor (Passchier, 1997) will be parallel to e_1 in the VPP.

When Eq. (26) is applied to this example, we obtain the torus illustrated on Fig. 16, with a converging point at $\dot{s}_x$ ($\dot{e}_2$) that represents the direction of the vorticity vector. This cyclide can be sliced into multiple circular sections, some with special significance as described above, which can be interpreted as a single Mohr-circle. Three of these sections are:

Fig. 16a shows the vorticity profile plane (VPP) corresponds to the basal cyclide circle, which contains the two eigenvectors and the two ISA normal to $\overrightarrow{w}$. This is the plane where structure asymmetry is more obvious and where shear sense should be gauged. This section of the cyclide is identical to the Mohr-circle for a 2D simplification and can be interpreted just in the same way.

Fig. 16b represents the flow plane (in the sense of Passchier, 1998), the eigenvector plane which contains the extensional (positive) eigenvalue. The boundary of a shear zone developed according to this flow type will be parallel to it. The flow plane can be considered, for practical reasons, the plane of foliation, where the lineation *L* can be observed and measured in the field. An eventual second lineation *L*′, will plot as a line in this section of the Mohr-cyclide.

Fig. 16c illustrates a plane which contains the vorticity vector, but lies at an angle with the eigenvectors and instantaneous stretching axes. This plane can represent, for instance, an "S-foliation" in a C + S pair, which can be used for shear sense determination. Sometimes it is possible to observe striations in these planes (e.g. Lin et al., 1998) that can give additional kinematic information. Such lines can also be represented in the Mohr-cyclide.

In summary, Mohr-cyclides, since they are not limited to 2D as Mohr-circles, allow the representation of multiple structural features in the same diagram. These may include different planes with geological meaning (or not), and all types of lineations included in them.

4. Summary

The graphical representation of second-rank tensors in three-dimensional Mohr-space are surfaces from the cyclide family, just as circles for second-rank tensors in 2D. The geometry of Mohr-cyclides is independent of reference frame and, therefore, these surfaces can be interpreted as Mohr diagrams. For any $\mathbf{T_{ij}}$ tensor, it is possible to define the same Mohr-cyclide from two independent approaches: analytical polar coordinates or via parametric equations. Mohr-cyclides are defined with respect to e_i, one of the eigenvectors of $\mathbf{T_{ij}}$; the relative magnitude of its eigenvalue defines the general shape of the surface, all of them with a converging point at e_i: (i) $e_i > e_j, e_k$-positive single-crescent cyclide; (ii) $e_i < e_j, e_k$-negative single-crescent cyclide; (iii) $e_j, e_k > e_i > e_j, e_k$-torus with a converging point. A Mohr-cyclide is a collection of Mohr-circles, corresponding to different orientations in space that may define a plane.

The concept of Mohr-cyclides is introduced in this paper with the examples of two tensors commonly used in Geology: the stress and flow tensors. Mohr-cyclides, however, are not exclusive of geological problems, as they represent a general property of all tensors, regardless of physical meaning. It is possible to define Mohr-cyclides for additional geological tensors, such as stretch and strain, as well as for other tensors used by all natural sciences.

Acknowledgements

This paper is a part of S.C.'s PhD thesis, funded with a scholarship (SFRH/12221/2003) provided by the Foundation for Science and Technology (FCT, Portugal). Caspar Visseveer helped to improve earlier drafts of this paper. We wish to thank Sue Treagus and Richard Lisle for thorough reviews.

Appendix A. Symbols and notations used in text

$\mathbf{T_{ij}}$	An unspecified tensor
T_{ij}	Tensor components
$\mathbf{R_{ij}}$	Rotation tensor
A, *B*, *C*, *D*, *E*	Cyclide parameters
θ, ψ	Cyclide angles (long, lat)
xx, *yy*, *zz*	General *xyz* reference frame (in text)
X_M,Y_M,Z_M	Coordinates of a point in Mohr space
i, *j*, *k*	(Subscripted) Unspecified components or reference frame
$\|$; $\perp$	Parallel to; orthogonal to
$\mathbf{S_{ij}}$	Stress tensor
σ_1, σ_2, σ_3	Principal stresses (max, int, min)
P, N_P	Plane *P*, pole to *P*
σ, σn, τ	Stress and its normal and shear components
σ_{nP}, τ_P	Normal and shear stress on *P*
φ	$\sigma \wedge \sigma_n$
S, N_S	Stress plane and its pole
δ	$N_S \wedge \sigma_1$
α	$N_P \wedge \sigma_1$
β	$N_P \wedge \sigma_2$
γ	$N_P \wedge \sigma_3$

$\mathbf{L_{ij}}$	Flow tensor
$e, \dot{e}$	Eigenvectors of $\mathbf{L_{ij}}$ (the flow apophysis), eigenvalues
$\mathbf{D_{ij}}$	Stretching rate tensor: stretching component of $\mathbf{L_{ij}}$
$\mathrm{ISA}_{1,2,3}$	Instantaneous stretching axes; eigenvectors of $\mathbf{D_{ij}}$
$\dot{s}_{1,2,3}$	Instantaneous stretching rates; eigenvalues of $\mathbf{D_{ij}}$
$\mathbf{W_{ij}}$	Vorticity tensor: rotational component of $\mathbf{L_{ij}}$
$\overrightarrow{w}; \overline{w}; w_i$	Vorticity vector with respect to ISA; its magnitude; its components
W_K	Sectional vorticity number
A_K	Sectional dilatancy number
T_K	Sectional extrusion number
$\dot{\omega}$	Rate of angular velocity
$\dot{s}$	Stretching rate at point m
$\overline{s}$	Mean stretching rate in the section normal to vorticity
$\mathbf{l_i}$	Lines of no instantaneous stretch
χ	$\mathbf{l_i} \wedge \mathbf{l_j}$ ($\cos\chi = A_K$)
υ	$e_j \wedge e_k$ ($\cos\upsilon = W_K$)
$\overrightarrow{m}$	Position vector of point m in the velocity field
$\overrightarrow{m}'$	Position vector of m after 1 unit of time
η_i	$\overrightarrow{m} \wedge \mathrm{ISA}_i$
$\dot{d}, \overline{d}$	rate of displacement vector, its magnitude
U	Pole of $\overrightarrow{m} - \dot{d}$ plane
φ	$\overrightarrow{m} \wedge \dot{d}$
δ	$U \wedge \overrightarrow{w}$ (parallel to one eigenvector)

Appendix B. Proof that the cyclides can be interpreted as Mohr diagrams

Means (1983) suggested that orthogonal lines in real space always plot as diameters of a Mohr-circle, irrespective of the components chosen to define the same tensor. In other words, considering the tensor rotation formula,

$$T'_{ij} = R_{ij} \cdot T_{ij} \cdot R^T_{ij} \tag{A1}$$

the Mohr-circle for $\mathbf{T'_{ij}}$ will be the same as for $\mathbf{T_{ij}}$, whichever angle θ is applied in the rotation tensor $\mathbf{R_{ij}}$. Take, for instance, a tensor of the form:

$$T_{ij} = \begin{vmatrix} a & b & 0 \\ c & d & 0 \\ 0 & 0 & f \end{vmatrix}$$

Lines parallel to the *xx*- and *yy*-reference axis in the geographical space plot give a circle P, defined by a centre Ctr and a diameter D:

$$Ctr_P \begin{cases} x : \dfrac{c-b}{2} \\ y : \dfrac{a+d}{2} \\ z : 0 \end{cases} \tag{A2}$$

$$D_p^2 = (a-d)^2 + (b+c)^2 \tag{A3}$$

From a rotation, we obtain alternative components for $\mathbf{T_{ij}}$,

$$a' = a\cos^2\theta + (b+c)\cos\theta\sin\theta + d\sin^2\theta$$

$$b' = b\cos^2\theta + (d-a)\cos\theta\sin\theta - c\sin^2\theta$$

$$c' = c\cos^2\theta + (d-a)\cos\theta\sin\theta - b\sin^2\theta$$

$$d' = d\cos^2\theta - (b+c)\cos\theta\sin\theta + a\sin^2\theta$$

$$f' = f \tag{A4}$$

which define an alternative circle P'. Substituting Eqs. (A4) in Eqs. (A2), the centre of circle P' is given by:

$$Ctr_{P'} \begin{cases} x : \dfrac{c(\cos^2\theta + \sin^2\theta) - b(\cos^2\theta + \sin^2\theta)}{2} \\ y : \dfrac{a(\cos^2\theta + \sin^2\theta) + d(\cos^2\theta + \sin^2\theta)}{2} \\ z : 0 \end{cases} \tag{A5}$$

With the fundamental rule of trigonometry it is clear that Eqs. (A2) and Eq. (A5) are identical. The diameter of circle P', after substitution of Eq. (A4) on Eq. (A3) and rather extensive use of the associative property of multiplications, can be written as:

$$D_{P'}^2 = (a-d)^2(\cos^2\theta + \sin^2\theta)^2 + (b+c)^2(\cos^2\theta + \sin^2\theta)^2 \tag{A6}$$

which is equal to the unprimed diameter (Eq. (A3)). Thus, it is safe to say that circles P and P' are one and the same, with equal diameter and centre coordinates, and that both represent a Mohr-circle.

The general proof for circles described above confirms that the basal circle in a Mohr-cyclide (e.g. Fig. 13a) is a Mohr-circle, but cannot be applied to the whole surface, because the cyclide geometry is more complex than a circle. To prove that a cyclide can be interpreted as a Mohr-diagram, it is necessary to recall an important property: the cyclide shape is defined by its parameters A, B, C, D (Shene, 2000), as well as parameter E and angle ρ (this work). With this in mind, it is possible to expand Means' proof for cyclides: *A cyclide will be a Mohr-diagram for T_{ij} if and only if its parameters A, B, C, D, E and ρ remain constant whatever combination of components is chosen from the infinite possibilities available to define T_{ij}*, which is equivalent to say that, *the Mohr-cyclide for T_{ij} is identical to the Mohr-cyclide for T'_{ij}*.

For an unspecified tensor $\mathbf{T_{ij}}$, with $f > a, d$, the cyclide parameters are given by the following formulas:

$$A = \sqrt{(E_y - f)^2 + E_x^2} \tag{A7}$$

$$B = \sqrt{A^2 - C^2} \tag{A8}$$

$$C = \frac{\sqrt{(b+c)^2+(a-d)^2}}{4} \tag{A9}$$

$$D = C \tag{A10}$$

$$E\begin{cases} E_x = \dfrac{c-b}{2} \\ E_y = \dfrac{a+d+2f}{4} \end{cases} \tag{A11}$$

$$\tan\rho = \frac{c-b}{a+d+2f} \quad \text{or} \quad \tan\rho = \frac{c-b}{a+d-2f} \tag{A12}$$

From this list, it is clear that only four parameters, A, C, E and ρ, are independent and necessary to prove the condition.

(I) *Parameter C*. Simple inspection of Eq. (A9) shows that $4C$ is given by an equation identical to the diameter of a circle (Eq. A3). Substituting Eq. (A4) in Eq. (A9) yields a result identical to Eq. (A3) and, thus: $\mathbf{4}\boldsymbol{C} = \mathbf{4}\boldsymbol{C}'$.

(II) *Parameter E*. Substituting Eq. (A4) in Eq. (A11) gives:

$$E\begin{cases} E_x = \dfrac{c\left(\cos^2\theta+\sin^2\theta\right) - b\left(\cos^2\theta+\sin^2\theta\right)}{2} \\ E_y = \dfrac{a\left(\cos^2\theta+\sin^2\theta\right) + d\left(\cos^2\theta+\sin^2\theta\right) + 2f}{4} \end{cases} \tag{A13}$$

Thus, $\mathrm{E} = \mathrm{E}'$

(III) *Parameter A*. From (II) and Eq. (A13), and taking into account that $f = f'$ (Eq. (A4)), it is clear that $\boldsymbol{A} = \boldsymbol{A}'$.

(IV) *Angle ρ*. Substituting Eq. (A4) in Eq. (A12) yields:

$$\tan\rho' = \frac{c\left(\cos^2\theta+\sin^2\theta\right) - b\left(\cos^2\theta+\sin^2\theta\right)}{a\left(\cos^2\theta+\sin^2\theta\right) + d\left(\cos^2\theta+\sin^2\theta\right) + 2f}$$

or

$$\tan\rho' = \frac{c\left(\cos^2\theta+\sin^2\theta\right) - b\left(\cos^2\theta+\sin^2\theta\right)}{a\left(\cos^2\theta+\sin^2\theta\right) + d\left(\cos^2\theta+\sin^2\theta\right) - 2f} \tag{A14}$$

And, therefore, $\rho = \rho'$.

From (I) to (IV), it is possible to conclude that the cyclide parameters are independent from any rotation applied to $\mathbf{T_{ij}}$. Thus, the cyclide remains the same whether defined by $\mathbf{T_{ij}}$ or $\mathbf{T'_{ij}}$ and can be interpreted as a Mohr-diagram. This is also consistent with the definition of a tensor as a mathematical entity independent of reference frame.

References

Allen, S., Dutta, D., 1997. Cyclides in pure blending I. Computer Aided Geometric Design 14, 51–75.

Angelier, J., 1979. Determination of the mean principal directions of stresses for a given fault population. Tectonophysics 56, T17–T26.

Brace, W.F., 1961. Mohr construction in the analysis of large geological strain. Geolological Society of America Bulletin 71, 1059–1080.

Bobyarchick, A.R., 1986. The eigenvalues of steady state flow in Mohr space. Tectonophysics 122, 35–51.

Delaney, P.T., Pollard, D.D., Zioney, J.I., MacKee, E.H., 1986. Field relations between dikes and joints: Emplacement processes and paleostress analysis. Journal of Geophysical Research 91, 4920–4938.

De Paor, D.G., Means, W.D., 1984. Mohr circles of the First and Second Kind and their use to represent tensor operations. Journal of Structural Geology 6, 693–701.

Dupin, C.P., 1822. Application de Géométrie et de Méchanique à la Marine, aux Ponts et Chaussées,etc. Bachelier, Paris.

Etchecopar, A., Vasseur, G., Daignieres, M., 1981. An inverse problem in microtectonics for the determination of stress tensors from fault striation analysis. Journal of Structural Geology 3, 51–65.

Iacopini, D., Passchier, C.W., Caruso, E., Köhn, D., 2007. Fabric attractors in triclinic flow systems and their application to high strain shear zones: A dynamical system approach. Journal of Structural Geology 29, 298–317.

Jiang, D., Williams, P.F., 1998. High strain zone: a unified model. Journal of Structural Geology 20, 1105–1120.

Jolly, R.J.H., Sanderson, D.J., 1997. A Mohr circle construction for the opening of a pre-existing fracture. Journal of Structural Geology 19, 887–892.

Lin, S., Jiang, D., Williams, P.F., 1998. Trans-pression (or transtension) zones of triclinic symmetry: natural example and theoretical modelling. In: Holdsworth, R.E., Strachan, R.A., Dewey, J.F. (Eds.), Continental Transpressional and Transtensional Tectonics. Geological Society of London, Special publications, vol. 135, pp. 41–57.

Lisle, R.J., 1979. The representation and calculation of the deviatoric component of the geological stress tensor. Journal of Structural Geology 1, 317–321.

Lisle, R.J., Ragan, D.M., 1988. Strain from three stretches—a simple Mohr circle solution. Journal of Structural Geology 10, 905–906.

Lister, G.S., Williams, P.F., 1983. The partitioning of deformation in flowing rock masses. Tectonophysics 92, 1–33.

Means, W.D., Hobbs, B.E., Lister, G.S., Williams, P.F., 1980. Vorticity and non-coaxiality in progressive deformations. Journal of Structural Geology 2, 371–378.

Means, W.D., 1982. An unfamiliar Mohr circle construction for finite strain. Tectonophysics 89, T1–T6.

Means, W.D., 1983. Application of the Mohr-circle construction to problems of inhomogeneous deformation. Journal of Structural Geology 5, 279–286.

Means, W.D., 1992. How to do anything with Mohr circles (except fry an egg). Unpublished manual of the short course presented at the Geological Society of America Meeting in Cincinnati, Ohio, October 1992.

Mohr, O., 1882. Über die Darstellung des Spannungszustandes und des Deformation-zustandes eines Körperelementes und über die Anwendung derselben in der Festigkeit-slehre. Civilingenieur 28, 113–115.

Nadai, A., 1950. Theory of Flow and Fracture of Solids. McGraw-Hill, New York.

Passchier, C.W., Urai, J.L., 1988. Vorticity and strain analysis using Mohr diagrams. Journal of Structural Geology 10, 755–763.

Passchier, C.W., 1986. Flow in natural shear zones—the consequences of spinning flow regimes. Earth and Planetary Science Letters 77, 70–80.

Passchier, C.W., 1987. Efficient use of the velocity gradient tensor in flow modelling. Tectonophysics 136, 159–163.

Passchier, C.W., 1988. The use of Mohr circles to describe non-coaxial progressive deformation. Tectonophysics 149, 323–338.

Passchier, C.W., 1990a. A Mohr circle construction to plot the stretch of material lines. Journal of Structural Geology 12, 513–515.

Passchier, C.W., 1990b. Reconstruction of deformation and flow parameters from deformed vein sets. Tectonophysics 180, 185–199.

Passchier, C.W., 1991. The classification of dilatant flow types. Journal of Structural Geology 13, 101–104.

Passchier, C.W., 1993. The sliding-scale Mohr diagram. Tectonophysics 218, 367–373.

Passchier, C.W., 1997. The fabric attractor. Journal of Structural Geology 19, 113–127.

Passchier, C.W., 1998. Monoclinic model shear zones. Journal of Structural Geology 20, 1121–1137.

Pratt, M.J., 1990. Cyclides in computer aided geometric design. Computer Aided Geometric Design 7, 221–242.

Ramberg, H., 1975. Particle paths, displacement and progressive strain applicable to rocks. Tectonophysics 28, 1–37.

Ramsay, J.G., 1967. Folding and Fracturing of Rocks. McGraw-Hill, New York.

Robin, P.-Y., Cruden, A.R., 1994. Strain and vorticity patterns in ideally ductile transpression zones. Journal of Structural Geology 16, 447–466.

Sanderson, D.J., Marchini, W.R.D., 1984. Transpression. Journal of Structural Geology 6, 449–458.

Shene, C.-K., 2000. Do blending and offsetting commute for Dupin cyclides? Computer Aided Geometric Design 17, 891–910.

Simpson, C., De Paor, D.G., 1993. Strain and kinematic analysis in general shear zones. Journal of Structural Geology 15, 1–20.

Spencer, A.J.M., 1980. Continuum Mechanics. Longman, London and New York.

Treagus, S.H., 1983. A theory of finite strain variation through contrasting layers, and its bearing on cleavage refraction. Journal of Structural Geology 5, 351–368.

Treagus, S.H., 1986. Some applications of the Mohr diagram for three-dimensional strain. Journal of Structural Geology 8, 819–830.

Treagus, S.H., 1990. The Mohr diagram for three-dimensional reciprocal stretch vs. rotation. Journal of Structural Geology 12, 383–395.

Vissers, R.L.M., 1994. Finite strain in simple shear, inspected with Mohr circles for stretch. Journal of Structural Geology 16, 1723–1726.

Wallis, S.R., 1992. Vorticity analysis in a metachert from the Sambagawa Belt, SW Japan. Journal of Structural Geology 14, 271–280.

Zhang, J., Zheng, Y., 1997. Polar Mohr constructions for strain analysis in general shear zones. Journal of Structural Geology 19, 745–748.